alteration so far reported in RCCC is the inactivation of the *VHL* gene. Loss of the VHL protein leads to an inappropriate accumulation of hypoxia-inducible mRNA, such as VEGF, which appears to be responsible for the hypervascular nature of RCCC.[4] Another characteristic and clinically important feature of RCCC is the high incidence of metastasis even in the relatively early stages of tumors. Disruption of the cell adhesion machinery is an initial step of cancer invasion and metastasis. In fact, in previous studies, it has been demonstrated that alterations of E-cadherin or integrins are frequently observed in RCCC.[5,6]

We previously identified a tumor suppressor gene, *CADM1/TSLC1*, in human nonsmall cell lung cancer (NSCLC).[7] The *CADM1* is expressed in most epithelial tissues, while its expression is frequently lost in many tumors, including NSCLC or prostate cancer.[8] CADM1 belongs to the immunoglobulin superfamily cell adhesion molecules and carries three immunoglobulin loops in the extracellular domain, a single transmembrane domain and a short cytoplasmic domain. Subsequent analysis has shown that CADM1 forms a unique subfamily within IgCAMs together with its homologous proteins, CADM2, CADM3 and CADM4, in which CADM2 and CADM3 are only expressed in the nerve systems.[9,10] We have reported that CADM4 is expressed in the brain, lung, large and small intestines and urinary organs and that CADM4 could act as a tumor suppressor in prostate cancer.[11]

We have also demonstrated that CADM1 associates with an actin-binding protein, 4.1B/DAL-1, through the FERM-binding motif in the cytoplasmic domain.[12] Frequent loss of 4.1B in lung adenocarcinoma, breast cancer and meningioma suggested that 4.1B could be a tumor suppressor.[13,14] 4.1B is a member of the 4.1-family proteins with 4.1R, 4.1N and 4.1G and shows significant homology with ezrin, radixin and moesin as well as merlin, which is the responsible gene product in neurofibromatosis type 2. In lung and breast cancer and meningioma, frequent abrogation of the cell adhesion machinery composed of CADM1 and 4.1B has been demonstrated.[15–19] In the mouse nephron, 4.1B is expressed in the proximal uriniferous tubules, while 4.1N is expressed in the distal tubules. On the other hand, 4.1R expression is only restricted to a portion of ascending limb of the loop of Henle, while no 4.1G expression is observed in the nephron.[20] Therefore, among the 4.1 family proteins, we chose 4.1B and 4.1N as possible molecules involved in renal tumorigenesis. In addition, we have previously demonstrated that 4.1B is frequently inactivated by promoter methylation, providing a prognostic factor in RCCC.[21] However, the normal partners of the membrane protein associated with 4.1B in RCCC have not been reported yet.

Here, we examined the tissue-specific expression of CADM4, CADM1, 4.1B and 4.1N proteins in human nephrons and demonstrated that CADM4 was expressed and interacted with 4.1B in human proximal uriniferous tubules that are the precursor cells of RCCC. The high incidence of loss of CADM4 expression in cell lines and primary tumors from RCCC, together with the suppressor activity in the tumorigenicity of RCC cells by CADM4, strongly suggests that CADM4 is a novel tumor suppressor candidate involved in RCCC in cooperation with 4.1B.

Material and methods

Cell lines

Human RCC cell lines, ACHN, 786-O and 769-P were obtained from the American Type Culture Collection (Rockville, MD); VMRC-RCW and Caki-1 cells, from the Japanese Collection of Research Bio-resources (Tokyo, Japan); OS-RC-2, RCC10RGB, TUHR4TKB, TUHR10TKB and TUHR14TKB cells, from the Riken Cell Bank (Tsukuba, Japan). Cells were cultured according to the suppliers' recommendations.

Surgical specimens

Forty pairs of cancerous and adjacent noncancerous tissues of RCCC were surgically resected at the University of Tokyo Hospital after written informed consent from each patient was obtained. Analyses of human materials were carried out according to the Guidelines of the Ethics Committee of the University of Tokyo (authorization No. 2566). Pathological diagnosis was performed by urological pathologists (A. G. and T. M.).

Antibodies

A rabbit polyclonal antibody (pAb) against CADM4/TSLL2 (Bc-2) was raised against 13 synthetic polypeptides of the C terminus of CADM1 coupled with keyhole limpet hemocyanin and purified with an affinity column (MBL, Nagoya, Japan) as described previously.[11] The CADM1 antibodies used in this study were two rabbit polyclonal antibodies (pAbs) against the cytoplasmic domain, C-18,[22] and number 6 and a chicken monoclonal antibody (mAb) against the ectodomain, 3E1.[23] A rabbit pAb against 4.1B/DAL-1 was described previously.[21] A mouse mAb against 4.1N and a goat pAb against GAPDH (V-18) were purchased from BD Biosciences (Franklin Lakes, NJ) and from Santa Cruz Biotechnology (Santa Cruz, CA), respectively.

Immunohistochemistry

Sequential sections of 4-μm thick from human RCCC and noncancerous kidney tissues of the same patients were cut from the paraffin blocks. The sections were deparaffinized, autoclaved in Histofine pH 9 (Nichirei Biosciences, Japan) at 121°C for 20 min, cooled down to room temperature and incubated with 0.3% H_2O_2/methanol for 30 min and with 5% normal donkey serum in 0.02% NaN_3/PBS for 30 min. These sections were incubated with the indicated primary antibodies and visualized by Envision kit/HRP (DAB) (Dako, Glostrup, Denmark) according to the manufacturer's recommendations. All sections were counterstained with hematoxylin. Elastica van Gieson (EVG) staining was also used to assess the vascular permeation of tumors.

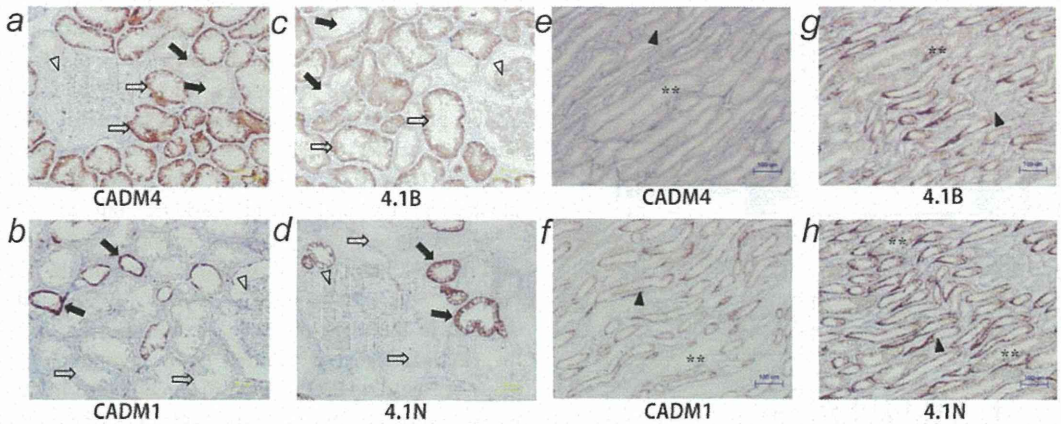

Figure 1. Immunohistochemical analyses of CADM4 (*a* and *e*), CADM1 (*b* and *f*), 4.1B (*c* and *g*) and 4.1N (*d* and *h*) proteins in normal human renal cortex (*a–d*) and medulla (*e–h*). Expression of CADM4 and 4.1B is detected in the proximal convoluted tubules (*a* and *c*), whereas that of CADM1 and 4.1N is detected in the distal convoluted tubules (*f* and *h*). Open and closed arrows indicate the proximal and the distal convoluted tubules, respectively, whereas open and closed arrowheads indicate the glomerulus and the loops of Henle, respectively. Asterisks and double asterisks indicate the collecting duct in the cortex and that in the medulla, respectively. The bar indicates 50 μm (*a–d*) or 100 μm (*e–h*).

Immunoprecipitation and Western blotting

Human RCCC and noncancerous renal tissues were treated with a lysis buffer [50 mM Tris–HCl, pH 7.5, 150 mM NaCl, 1% Triton X-100, 1 mM EDTA, 10 mM NaF, 1 mM Na_3VO_4] with protease inhibitors [200 μM AEBSF, 10 μM leupeptin, 1 μM pepstatin A] and centrifuged at 3,000 rpm at 4°C for 10 min to obtain the tissue lysates as the supernatants. For direct Western blotting, an aliquot of the tissue lysates (1 μg) was applied in each lane in a 4–12% gradient SDS–PAGE (Invitrogen, Carlsbad, CA). For immunoprecipitation, an aliquot of tissue lysates (1–2 mg) was incubated with an appropriate primary antibody for 30 min at 4°C, and then protein A-Sepharose 6MB (GE Healthcare, Buckinghamshire, UK) was added and further incubated for overnight at 4°C. Immunoprecipitates were rinsed with the lysis buffer three times, suspended in a sample buffer containing 2% SDS and incubated for 5 min at 100°C. The samples were fractionated in 4–12% gradient SDS–PAGE, transferred to a polyvinylidene difluoride membrane (Millipore, Bedford, MA) and incubated with an appropriate primary antibody. The binding of the primary antibody was detected with ECL™ Western Blotting Detection Reagent (GE Healthcare) using a peroxidase-conjugated secondary antibody (GE Healthcare).

Reverse-transcription PCR

Total cellular RNA was extracted from 786-O cells using an RNeasy Mini kit (QIAGEN, Valencia, CA). One microgram of total cellular RNA was reverse-transcribed using Superscript II reverse transcriptase (Invitrogen) with oligo(dT) primers. A CADM4 fragment of 128 bp was amplified using 0.5 μmol/l of primers 5′-TAGTGGGCATGGTCTGGTG-3′ and 5′-TTTCC TCTTGTGTCCGTCG-3′. A 4.1B fragment of 153 bp was amplified using 0.5 μmol/l of primers 5′-GTAGTGGTCCATA AAGAGACAGAGA-3′ and 5′-GATACAAGTCAGTTGGGT TAGAAGA-3′, whereas a β-actin fragment of 646 bp was amplified using 0.1 μmol/l primers 5′-AAATCTGGCACCA CACCTT-3′ and 5′-AGCACTGTGTTGGCGTACAG-3′.

Restoration of CADM4 expression by 5-aza-2′-deoxycytidine

About 1×10^5 of 786-O cells were seeded at day 0, treated with 5-aza-2′-deoxycytidine (5-aza-CdR; 10 μM; Sigma-Aldrich, St., MO) or PBS as a control for 24 hr on days 2 and 5 and collected on day 8 as reported previously.[7,24]

Expression of CADM4 in an RCC cell line

A vector expressing the whole-coding sequence of human CADM4 (pcTSLL2/CADM4) was described previously.[11] 786-O cells were transfected with a pcTSLL2/CADM4 or an empty vector, pcDNA3.1 (Invitrogen) using Lipofectamine LTX (Invitrogen) according to the manufacturer's instructions, selected against 500 μg/ml G418 sulfate (Invitrogen) and three independent cell clones were then obtained.

Tumorigenicity analysis

A suspension of 1×10^5 cells in 0.2 ml of PBS was injected subcutaneously into one to two sites on the backs of 6-week female BALB/c nu/nu mice. Tumor growth was assessed by measuring the xenografts in two dimensions twice a week. Tumor volumes were calculated according to the formula (volume) = 1/2 × (long axis) × (short axis).[2] All animal

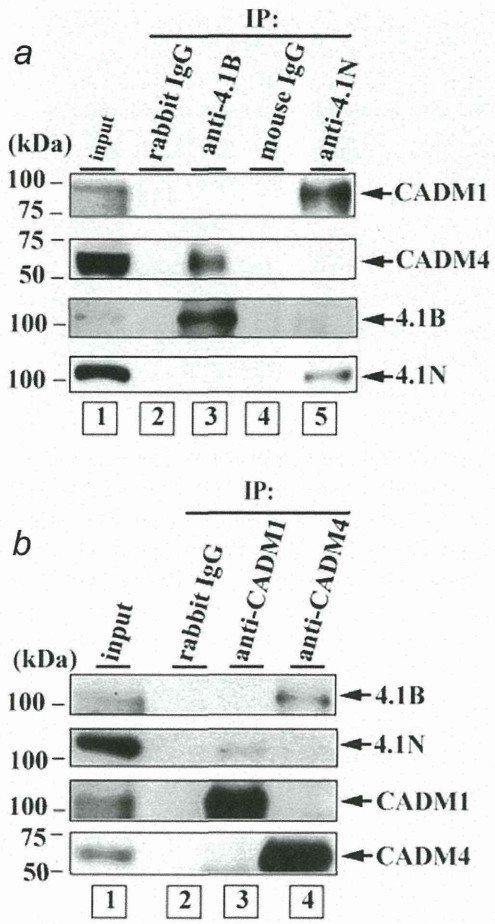

Figure 2. Interaction of CADM4 with 4.1B and CADM1 with 4.1N. (*a*) Total lysates of normal human kidney were immunoprecipitated with control rabbit IgG (lane 2), anti-4.1B pAb (lane 3), control mouse IgG (lane 4) and anti-4.1N pAb (lane 5), and binding proteins were detected by immunoblotting using anti-CADM1 pAb, anti-CADM4 pAb, anti-4.1B pAb and anti-4.1N pAb (top to bottom). An aliquot of the tissue lysates (5 μg) was loaded as a control (lane 1). (*b*) Total lysates of normal human kidney were immunoprecipitated with control rabbit IgG (lane 2), anti-CADM1 pAb (lane 3) and anti-CADM4 pAb (lane 4), and binding proteins were detected by immunoblotting using anti-4.1B pAb, anti-4.1N pAb, anti-CADM1 pAb and amti-CADM4 pAb (top to bottom). An aliquot of the tissue lysates (5 μg) was loaded as a control (lane 1).

experiments were performed in accordance with the institutional guidelines.

Results

Cell-type-specific expression of the CADM- and 4.1-family proteins in human kidney

To understand the physiological and pathological roles of these proteins in the kidney, precise patterns of expression were examined in human normal kidneys by immmunohistochemical staining using specific antibodies against CADM1, CADM4, 4.1B and 4.1N. As shown in Figure 1*a*, CADM4 is specifically expressed at the cell–cell attachment sites in the proximal convoluted tubules. 4.1B is also expressed along the cell membrane in the proximal tubules as reported previously (Fig. 1*c*).[20,21] However, neither CADM1 nor 4.1N gives any signals in the proximal tubules (Figs. 1*b* and 1*d*). In the distal convoluted tubules, on the other hand, CADM1, but not CADM4, is expressed along the cell membrane (Figs. 1*a* and 1*b*). Expression of 4.1N, but not 4.1B, is also detected in the distal tubules (Figs. 1*c* and 1*d*). In addition, signals of 4.1B and 4.1N are detected in the loops of Henle or the collecting ducts, whereas the CADM1 signal is detected in the ascending limbs of the loops of Henle. 4.1B expression is also observed in the glomerulus as reported previously.[21] In contrast, CADM4 is expressed exclusively in human proximal tubules as summarized in Supporting Information Table 1. Taken together, the findings clearly indicate that CADM4 and 4.1B are expressed in the proximal tubules, while CADM1 and 4.1N are expressed in the distal tubules in human kidney.

Interaction of CADM4 and 4.1B protein

CADM1 associates with 4.1B through its FERM-binding motif in normal epithelial tissues.[12] Coincident expression of CADM4 and 4.1B in the proximal tubules and that of CADM1 and 4.1N in the distal tubules prompted us to examine the possible association of each pair of proteins by immunoprecipitation coupled with Western blotting. As shown in Figure 2*a*, when the lysate of normal human kidney was immunoprecipitated with an antibody against 4.1B and immunoblotted with an anti-CADM4 antibody, specific signals of about 55 kDa corresponding to CADM4 were detected (Fig. 2*a*, lane 3). However, no CADM1 protein was coprecipitated when the same immunoprecipitate was blotted with an anti-CADM1 antibody (Fig. 2*a*, lane 3). Inversely, when normal kidney lysate was immunoprecipitated with an anti-CADM4 antibody and immunoblotted with an anti-4.1B antibody, distinct signals corresponding to 4.1B were detected (Fig. 2*b*, lane 4). However, no 4.1N protein was coprecipitated with CADM4 (Fig. 2*b*, lane 4). On the other hand, when normal kidney lysate was immunoprecipitated with an anti-4.1N antibody and then immune-blotted with an anti-CADM1 antibody, CADM1 signals were detected (Fig. 2*a*, lane 5). However, no CADM4 protein was co-immunoprecipitated with 4.1N. Moreover, 4.1N, but not 4.1B, was inversely co-immunoprecipitated with an anti-CADM1 antibody (Fig. 2*b*, lane 3). These results indicate that CADM4 associates with 4.1B, while CADM1 associates with 4.1N in normal human kidney cells, corresponding to the pattern of their tissue-specific expression.

Frequent loss of CADM4 and 4.1B expression in human RCC cells and RCCC tumors

Because RCCC is derived from the proximal uriniferous tubules, possible alteration in the expression of CADM4 as well as 4.1B was examined by Western blotting. As shown in

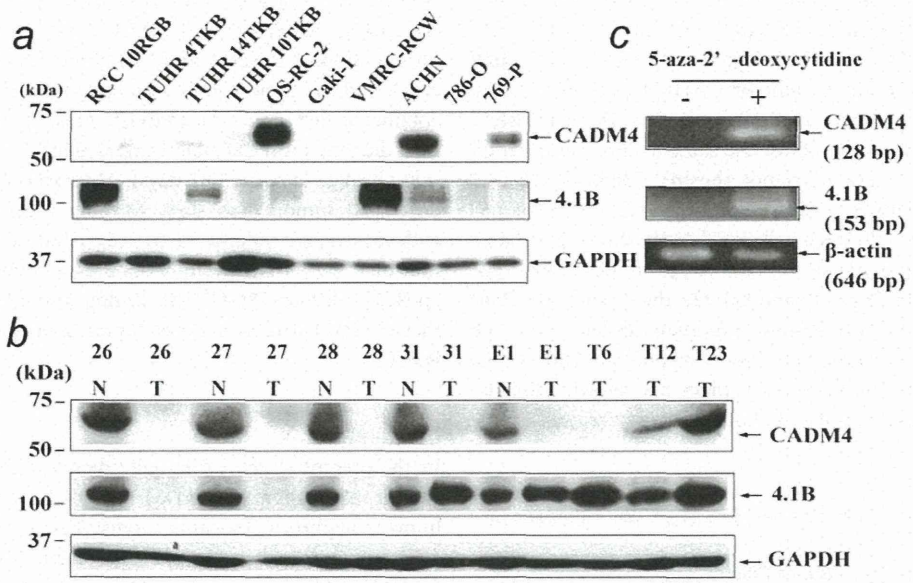

Figure 3. Loss of expression of CADM4 and 4.1B proteins in RCCC and restoration of CADM4 expression by 5-aza-2′-deoxycytidine. (*a* and *b*) Immunoblotting of CADM4 and 4.1B proteins in 10 RCC cell lines (*a*) and the primary tumors of RCCC (*b*). An aliquot of the tissue lysates (1 μg) was subjected to 4–12% SDS–PAGE and detected by anti-CADM4 pAb (upper), anti-4.1B pAb (middle) and anti-GAPDH mAb as a control (lower). N and T in (*b*) indicate noncancerous renal tissues and tumor tissues, respectively, whereas the number indicates individual patients. (*c*) Reverse transcriptase-PCR analysis of the CADM4 (upper), 4.1B (middle) and beta-actin as a control (lower) in 786-O cells treated with or without 5-aza-2′ deoxycytidine.

Figure 3*a*, 7 of 10 (70%) RCC cell lines showed loss or marked reduction in CADM4 expression. In addition, 6 of 10 (60%) from the same panel of RCC cells lost or markedly reduced 4.1B expression. In total, 9 of 10 (90%) RCC cells lost either CADM4 or 4.1B expression, suggesting that the disruption of the CADM4-4.1B cascade is an extremely frequent event in RCC. We have previously shown that 4.1B is inactivated by methylation of the gene promoter in RCCC. Therefore, to examine the possible involvement of promoter methylation in silencing of the *CADM4* gene, 786-O cells completely lacking CADM4 expression were treated with 5-aza-2′ deoxycytidine for 24 hr twice as described in Material and methods section. As shown in Figure 3*c*, CADM4 mRNA was restored in 786-O cells, suggesting that promoter methylation could be involved in at least a subset of RCC cell lines.

Next, we examined the expression of CADM4 in primary RCCC surgically resected and pathologically diagnosed at the University of Tokyo Hospital. Western blotting revealed that 28 of 40 (70%) primary RCCC lost CADM4 expression, while noncancerous renal tissues from the same patients expressed a significant amount of CADM4 protein (Fig. 3*b*). Loss of CADM4 expression was observed at high frequency even in RCCC at relatively early stages, including 10 of 16 (68%) tumors with T1a or 5 of 6 (83%) tumors with Fuhrman's grade 1. Interestingly, CADM4 expression was preferentially lost in RCCC with vascular infiltration (15/17, 88%) relative to those without vascular infiltration (13/23, 57%; $p = 0.04$; Table 1). These findings suggest that loss of CADM4 is a relatively early event in renal tumorigenesis and could be involved in vascular infiltration. Histological features are shown in Supporting Information Figure 1 for tumors with and without CADM4 expression. In tumors lacking CADM4 expression, inconspicuous vascular infiltrations (Supporting Information Figs. 1*a* and 1*c*) were manifested by EVG stain in large- and small-sized veins (Supporting Information Figs. 1*b* and 1*d*). In contrast, vascular infiltration was not identified even by EVG stain in tumors expressing CADM4 (Supporting Information Figs. 1*e* and 1*f*). In addition to CADM4, loss of 4.1B expression was detected in 19 of 40 (48%) primary RCCC by Western blotting (Fig. 3*b*). In total, the loss of expression of CADM4 or 4.1B occurred in 32 of 40 (80%) of RCCC. Interestingly, average size of the tumors lacking expression of either CADM4 or 4.1B or both was significantly larger than that of the tumors expressing both CADM4 and 4.1B ($p = 0.028$) (Table 2). No pathological changes, however, were observed between the tumors lacking both CADM4 and 4.1B and those lacking either of them, supporting an idea that CADM4 and 4.1B proteins act in the same cascade of cell adhesion.

Suppression of tumorigenicity of an RCC cell line, 786-O, by CADM4

To understand the biological function of CADM4 in RCCC, we transfected a CADM4 expression vector into an RCC cell

line, 786-O, completely lacking endogenous CADM4 expression, and obtained three independent transfectants (786/CADM4-1~3). As shown in Figure 4*a*, these cells stably expressed a significant amount of CADM4 protein. On the other hand, the amounts of 4.1B protein in these transfectants were quite low and almost the same as those in parental 786-O and 786/V cells (data not shown). 786/CADM4-1~3 cells showed essentially similar morphology to 786/V or parental 786-O cells, although cell populations showing a flatter morphology appeared to be more prominent in 786/CADM4-1~3 cells (Figs. 4*b* and 4*c*). On the other hand, 786/CADM4-1~3 cells did not show a dramatic difference in cell proliferation *in vitro* relative to 786/V or parental 786-O cells when analyzed by an MTS assay (data not shown). Finally, the tumor-forming activity of these cells *in vivo* was examined by injecting them into the back of BALB/c nu/nu mice. As shown in Figure 4*d*, 786/V cells developed palpable tumors around 3 weeks after injection (average latency: 17.2 days), and the tumors grew into large tumors with an average volume of 268 mm^3. In contrast, most of the 786/CADM4 cells did not form palpable tumors until 4 weeks after injection (average latency: 33.1 days). Moreover, the growth of the developed tumors was slow, forming much smaller masses with an average volume of 21 mm^3, indicating that restoration of CADM4 significantly suppresses tumor formation by an RCC cell line, 786-O. This finding provides more evidence that CADM4 acts as a novel tumor suppressor candidate in RCCC.

Table 1. Pathological parameters and loss of CADM4 expression in RCCC

Parameters	No. of Tumors Lost CADM4/No. of Tumors Examined (%)	
T-Classification		
1a	10/16 (63)	NS
1b	9/13 (69)	
2	2/3 (67)	
3a	3/4 (75)	
3b	4/4 (100)	
Fuhrman's Grade		
1	5/6 (83)	NS
2	16/24 (67)	
3	7/9 (78)	
4	0/1 (0)	
Vascular Infiltration		
(−)	13/23 (57)	*
(+)	15/17(88)	

*$p = 0.04$.
NS: not significant.

Discussion

In the present study, we initially demonstrated the cell-type-specific expression of CADM- and 4.1- family proteins in human nephrons by immunohistohemistry. CADM4 and 4.1B are expressed in the proximal uriniferous tubules, while CADM1 and 4.1N are expressed in the distal tubules. Such distinct patterns of expression have not been reported in other organs, including the lung, where CADM1, CADM4, 4.1B and 4.1N are all expressed in the pulmonary epithelial cells. Cell-type-specific expression of these proteins in the nephron, therefore, suggests that the cell adhesion machinery of CADM- and 4.1- proteins might play specific roles in each uriniferous tubule, for example, those related to the ion transport or re-absorption of specific molecules, although some of these proteins are also expressed in the loops of Henle or the collecting ducts in human kidney (Fig. 1). Next, by immunoprecipitation analysis coupled with Western blotting, we demonstrated that the CADM4 protein associated with 4.1B, while CADM1 associated with 4.1N in normal human kidney. Previous studies have reported that CADM1 associates with 4.1B through the FERM-binding motif in epithelial cells.[12] In addition, CADM3 is shown to associate with 4.1N in neuronal cells.[25] These results suggest that both CADM1 and CADM4 molecules have the potential to associate with both 4.1B and 4.1N. However, the clear demonstration in the present study of the specific interaction between

Table 2. Expression status of CADM4 and 4.1B and pathological characters of RCCC

Expression Status of CADM4/4.1B	No. of Tumors	Average Size (mm^3)	No. of Tumors (%) with T1		Vascular Infiltration		Metastasis	
+/+	8	40 ± 1	7 (88)	NS	1(13)	NS	0 (0)	
+/− and −/+	17	62 ± 33	9 (53)		11 (65)		3 (18)	
−/−	15	49 ± 24	9 (60)		5 (33)		3 (20)	
Total	40	53 ± 28	25 (63)		17 (43)		6 (15)	

*$p = 0.028$.
NS: not significant.

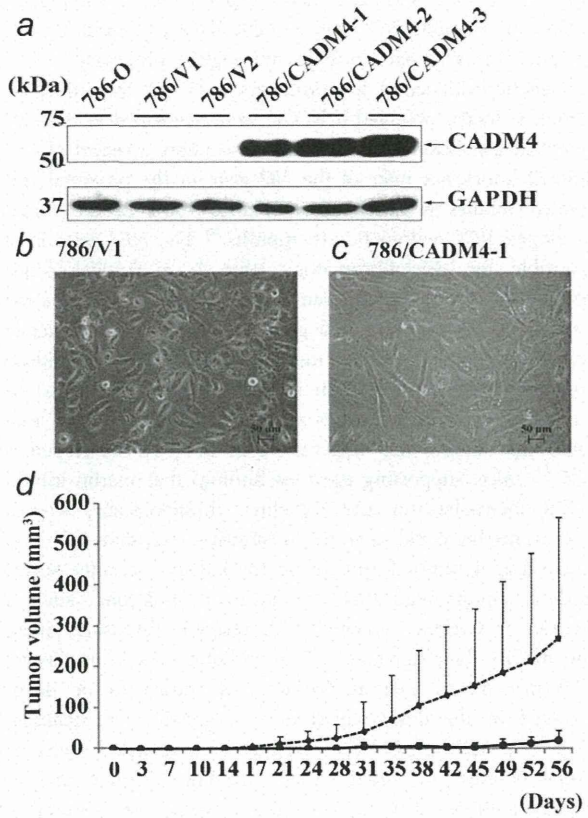

Figure 4. Suppression of tumorigenicity of 786-O cells in nude mice by CADM4. (*a*) Western blotting of CADM4 protein (upper) and control GAPDH protein (lower) in parental 786-O cells, 786-O cell clones transfected with a vector alone (786/V1, 786/V2) and 786-O cell clones transfected with CADM4 (786/CADM4-1, 786/CADM4-2 and 786/CADM4-3). (*b* and *c*) Morphology of 786/V1 (*b*) and 786/CADM4-1 (*c*) cells under phase-contrast microscopy. The bar indicates 50 μm. Original magnification, ×100. (*d*) Tumor formation in nude mice. The average volume of tumors that formed at 18 sites was determined at the indicated times after injection of 10^5 cells from the 786/V (dashed line) and 786/CADM4 (solid line) cells. $*p = 0.00012$.

CADM4 and 4.1B and between CADM1 and 4.1N in human kidney lysates strongly supports the finding that CADM4 and 4.1B are co-expressed in the proximal tubules while CADM1 and 4.1N are coexpressed in the distal tubules.

In the previously study, we have shown the frequent inactivation of 4.1B in RCCC.[21] Therefore, in this study, we examined whether CADM4 could also act as a tumor suppressor in RCCC. This hypothesis was supported by two lines of evidence (1) the frequent loss of CADM4 expression in primary tumors and cell lines from RCCC and (2) the suppression of the suppression of subcutaneous tumor formation of a human RCC cell line, 786-O, in nude mice by the introduction of CADM4. It is quite noteworthy that over 70% of primary RCCC tumors lost CADM4 expression in Western blotting or immunohistochemistry. The loss of CADM4 is, therefore, one of the most frequent molecular alterations so far reported in RCCC. It is well known that the *VHL* gene is inactivated in about 80% of RCCC.[26] However, mutation of the *VHL* and inactivation of the CADM4-4.1B cascade appears to be independent at least in 7 RCC cell lines with characterized VHL status as summarized in Supporting Information Table 2. This finding could be consistent with possible distinct functions of a cell adhesion molecule, CADM4 and a transcriptional silencer, VHL, although mutation of the *VHL* in 40 primary RCCCs remains to be examined. The clinicopathological features of the tumors revealed that loss of CADM4 expression already occurred in the early stage of RCCC tumors with T1a or Fuhrman's grade 1, suggesting that loss of CADM4 is a relatively early event in renal carcinogenesis. A more important finding is the significant association of the loss of CADM4 with the vascular infiltration of RCCC. Considerable portions of RCCC, especially a subset of those successfully resected by surgical operation, often contain the lesions of vascular infiltration, which is known to provide one of the prognostic markers of an RCCC patient.[27] Tumors lacking CADM4 expression might have the potential to metastasize to the distant organs through vascular infiltration, even though the relevant tumors are in the early clinicopathological stages on the basis of the TNM classification. Further studies as to the recurrence of RCCC in these patients would be required to answer this hypothesis.

Tumor-forming activity in nude mice has been considered to be the classic and most established criteria to assess the malignant phenotype of cultured cancer cells. On the basis of this criterion, 786-O is a malignant RCC cell for its tumorigenicity in nude mice as reported previously.[28] In this study, CADM4 appears to suppress tumor growth, as shown in Figure 4*d*, where the average volume of developed tumors at 56 days from 786/CADM4 cells (21 mm^3) is much smaller than that from 786/V cells (268 mm^3). Moreover, tumorigenicity in nude mice was recently re-evaluated as a method to assess the stemness of cancer cells. From this point of view, 786-O cells appear to contain a considerable number of cancer stem cells, because tumors developed in all 18 injection sites of 10^5 of 786/V cells with a relatively short latency averaging 17.2 days. In contrast, the restoration of CADM4 expression appears to decrease the subpopulation of cancer stem cells, because 10^5 of 786/CADM4 cells failed to develop tumors in 4 of 18 injection sites even at 56 days after injection. Moreover, the average latency of tumor formation was 33.1 days, much longer than that in 786/V cells. These results suggest that CADM4 suppresses not only the tumor growth but also the size of the cancer stem cell population in 786-O cells. However, these tumors only grew locally at the injected sites, and none of the tumors showed invasion or metastasis to adjacent or distant organs until 56 days after injection. These results suggest that even 786/V cells did not recapitulate the vascular infiltration of human RCCC in nude mouse-model, although we did not confirm absence of the vascular infiltration in these tumors.

It has been reported that 4.1B, Timp-3, RASSF1 and several other tumor suppressor genes are inactivated by promoter

methylation at high frequency in RCCC.[21,29–31] In this study, treatment of RCC cells with 5-aza-2′ deoxycytidine restored CADM4 expression in 786-O cells lacking endogenous CADM4 expression, suggesting that promoter methylation is involved in at least a portion of RCCC. We failed, however, to examine the detailed state of the *CADM4* gene promoter in RCC cell lines or primary RCCC by bisulfate sequencing or the COBRA method probably due to the extraordinary CpG-rich structure of the *CADM4* gene promoter. Therefore, the molecular cause of the aberration of CADM4 molecule in primary RCCC remains to be elucidated. In addition to the promoter methylation, loss of heterozygosity (LOH) on 19q13.2, where the *CADM4* gene is mapped, could be involved as observed in many other tumor suppressor genes, including the *CADM1*.[32] Inactivating mutations, including point mutations, frameshift and insertions/deletions might be additional molecular mechanisms to inactivate the *CADM4* gene, although inactivation through such mechanisms is relatively rare in the case of the *CADM1*.[33] It is interesting that chromosomal region 19q13, on which the *CADM4* gene is localized, also show LOH frequently in gliomas, suggesting that a similar mechanism connected to cell adhesion could play a role in neurogenic tumorigenesis.[34,35] On the other hand, 4.1B expression was lost in about one half of RCCC as we reported previously.[21] In this study, we confirmed using a distinct series of samples that 48% of primary RCCC tumors showed loss or marked reduction of 4.1B expression. In total, 32 of 40 (80%) primary RCCC showed loss or marked reduction of either CADM4 or 4.1B, indicating that disruption of the CADM4-4.1B cascade is one of the most frequent events in RCCC. We have previously reported that CADM4 could be a tumor suppressor candidate in prostate cancer on the basis of the frequent loss of CADM4 expression (6 of 9) in primary prostate cancer as well as the suppression of tumor-forming activity by CADM4 in a prostate cancer cell line, PPC-1.[11] As shown previously, CADM4 is expressed in a quite unique spectrum of tissues, such as the brain, lung, large and small intestines and urinary organs, including the kidney, ureter, bladder and prostate. The involvement of CADM4 in both RCCC and prostate cancer suggests that the malignant tumors of uroepithelial origin might have a common target cascade, at least in part, in their carcinogenic processes.

Genetic evidence of the involvement of CADM4 in RCCC would be finally obtained if RCCC were developed in mice deficient in the *Cadm4* gene. In this connection, a report of conditional knock-out mice of the *Nf2* gene in the proximal convoluted tubules is noteworthy, because 100% of these mice developed RCC within 6 - 10 months.[36] The *NF2* gene is responsible for neurofibromatosis type 2, a familial cancer affected by bilateral eighth-cranial-nerve tumors, as well as meningiomas, shwannomas and gliomas. The *NF2* gene encodes an actin-binding protein, merlin, which shows significant homology with ezrin, radixin and moesin, in addition to the 4.1 family proteins.[37] Further analyses by Morris *et al.*[33] indicated that EGFR was hyperactivated in RCC developed in $Nf2^{-/-}$ mice, supporting previous findings that merlin inhibits EGFR internalization and signaling physiologically, whereas loss of merlin could lead to constitutive activation of EGFR and resultant tumor formation in the kidney. Recently, several studies demonstrated that cell adhesion molecules, such as NCAM or CADM1, interact with receptor thyrosine kinases and modify their signaling.[38,39] In addition, loss of merlin and 4.1B protein, as well as CADM1, is shown to be deeply involved in the development and progression of meningiomas.[14,40] CADM4 could also associate with several receptor tyrosine kinases and modify their signaling. Further analyses, including those of $Cadm4^{-/-}$ mice, would be required to understand the role of CADM4 in human renal carcinogenesis.

Acknowledgements

We are grateful to Ms. Hiromi Ichihara, Ms. Tomoko Masuda and Ms. Keiko Kimura for their technical assistance and to Ms. Seiko Iwata for her secretarial assistance. A Grant-in-Aid for Scientific Research (B) [for Y.M.] and a Grant-in-Aid for Young Scientists (B) [for M.SY.] from the Ministry of Education, Culture, Sports, Science, and Technology, Japan; a Grant-in-Aid for the Third Term Comprehensive Control Research for Cancer from the Ministry of Health, Labor, and Welfare, Japan (Y.M.); and a Grant for the Promotion of Fundamental Studies in Health Sciences from the National Institute of Biomedical Innovation (for Y.M.)

References

1. Ferlay J, Shin HR, Bray F, Forman D, Mathers C, Parkin DM. Estimates of worldwide burden of cancer in 2008: GLOBOCAN 2008. *Int J Cancer* 2010;127: 2918–27.
2. Motzer RJ, Bander NH, Nanus DM. Renal-cell carcinoma. *N Engl J Med* 1996;335: 865–75.
3. Linehan WM, Walther MM, Zbar B. The genetic basis of cancer of the kidney. *J Urol* 2003;170:2163–72.
4. Kondo K, Yao M, Yoshida MS, Kishida T, Shuin T, Miura T, Moriyama M, Kobayashi K, Sasaki N, Kaneo S, Kawakami S, Baba M, et al. Comprehensive mutational analysis of the VHL gene in sporadic renal cell carcinoma: relationship to clinicopathological parameters. *Genes Chromosomes Cancer* 2002;34:58–68.
5. Russell RC, Ohh M. The role of VHL in the regulation of E-cadherin: a new connection in an old pathway. *Cell Cycle* 2007;6:56–9.
6. Miyoshi J, Takai Y. Nectin and nectin-like molecules: biology and pathology. *Am J Nephrol* 2007;27:590–604.
7. Kuramochi M, Fukuhara H, Nobukuni T, Kanbe T, Maruyama T, Ghosh HP, Pletcher M, Isomura M, Onizuka M, Kitamura T, Sekiya T, Reeves RH, Murakami Y. TSLC1 is a tumor-suppressor gene in human non-small-cell lung cancer. *Nat Genet* 2001;27:427–30.
8. Fukuhara H, Kuramochi M, Fukami T, Kasahara K, Furuhata M, Nobukuni T, Maruyama T, Isogai K, Sekiya T, Shuin T, Kitamura T, Reeves RH, et al. Promoter methylation of the TSLC1 and tumor suppression by its gene product in human prostate cancer. *Jpn J Cancer Res* 2002;93:605–9.
9. Fukuhara H, Kuramochi M, Nobukuni T, Fukami T, Saino M, Maruyama T, Nomura S, Sekiya T, Murakami Y. Isolation of the TSLL1 and TSLL2 genes, members of the tumor suppressor TSLC1 gene family encoding transmembrane proteins. *Oncogene* 2001; 20:5401–7.
10. Biederer T. Bioinformatic characterization of the SynCAM family of immunoglobulin-

like domain-containing adhesion molecules. *Genomics* 2006;87:139–50.
11. Williams YN, Masuda M, Sakurai-Yageta M, Maruyama T, Shibuya M, Murakami Y. Cell adhesion and prostate tumor suppressor activity of TSLL2/IGSF4C, an immunoglobulin superfamily molecule homologous to TSLC1/IGSF4. *Oncogene* 2006;25:1446–53.
12. Yageta M, Kuramochi M, Masuda M, Fukami T, Fukuhara H, Maruyama T, Shibuya M, Murakami Y. Direct association of TSLC1 and DAL-1, two distinct tumor suppressor proteins in lung cancer. *Cancer Res* 2002;62:5129–33.
13. Tran YK, Bogler O, Gorse KM, Wieland I, Green MR, Newsham IF. A novel meber of the NF2/ERM/4.1 superfamily with growth suppressing properties in lung cancer. *Cancer Res* 1999;59:35–43.
14. Gutmann DH, Donahoe J, Perry A, Lemke N, Karen G, Kittiniyom K, Rempel AS, Gutierrez AJ, Newsham FI. Loss of DAL-1, a protein 4.1-related tumor suppressor, is an important early event in the pathogenesis of meningiomas. *Hum Mol Genet* 2000;9:1495–500.
15. Kikuchi S, Yamada D, Fukami T, Masuda M, Sakurai-Yageta M, Williams YN, Maruyama T, Asamura H, Matsuno Y, Onizuka M, Murakami Y. Promoter methylation of the DAL-1/4.1B predicts poor prognosis in non-small cell lung cancer. *Clin Cancer Res* 2005;11:2954–61.
16. Kikuchi S, Yamada D, Fukami T, Maruyama T, Ito A, Asamura H, Matsuno Y, Onizuka M, Murakami Y. Hypermethylation of the TSLC1/IGSF4 promoter is associated with tobacco smoking and a poor prognosis in primary non-small cell lung cancer. *Cancer* 2006; 106:1751–8.
17. Heller G, Fong KM, Girard L, Seidl S, End-Pfützenreuter A, Lang G, Gazdar AF, Minna JD, Zielinski CC, Zöchbauer-Müller S. Expression and methylation pattern of TSLC1 cascade genes in lung carcinomas. *Oncogene* 2006;25:959–68.
18. Heller G, Geradts J, Ziegler B, Newsham I, Filipits M, Markis-Ritzinger EM, Kandioler D, Berger W, Stiglbauer W, Depisch D, Pirker R, Zielinski CC, et al. Downregulation of TSLC1 and DAL-1 expression occurs frequently in breast cancer. *Breast Cancer Res Treat* 2007;103: 283–91.
19. Lusis E, Gutmann DH. Meningioma: an update. *Curr Opin Neurol* 2004;17:687–92.
20. Ramez M, Blot-Chabaud M, Cluzeaud F, Chanan S, Patterson M, Walensky LD, Marfatia S, Baines AJ, Chasis JA, Conboy JG, Mohandas N, Gascard P. Distinct distribution of specific members of protein 4.1 gene family in the mouse nephron. *Kidney Int* 2003;63:1321–37.
21. Yamada D, Kikuchi S, Williams YN, Sakurai-Yageta M, Masuda M, Maruyama T, Tomita K, Gutmann DH, Kakizoe T, Kitamura T, Murakami Y. Promoter hypermethylation of the potential tumor suppressor DAL-1/4.1B gene in renal clear cell carcinoma. *Int J Cancer* 2006;118: 916–23.
22. Sakurai-Yageta M, Masuda M, Tsuboi Y, Ito A, Murakami Y. Tumor suppressor CADM1 is involved in epithelial cell structure. *Biochem Biophys Res Commun* 2009;90:977–82.
23. Koma Y, Furuno T, Hagiyama M, Hamaguchi K, Nakanishi M, Masuda M, Hirota S, Yokozaki H, Ito A. Cell adhesion molecule 1 is a novel pancreatic-islet cell adhesion molecule that mediates nerve-islet cell interactions. *Gastroenterology* 2008;134: 1544–54.
24. Veigl ML, Kasturi L, Olechnowicz J, Ma AH, Lutterbaugh JD, Periyasamy S, Li GM, Drummond J, Modrich PL, Sedwick WD, Markowitz SD. Bialleic inactivation of hMLH1 by epigenetic gene silencing, a novel mechanism causing human MSI cancers. *Proc Natl Acad Sci USA* 1998;95: 8698–702.
25. Zhou Y, Du G, Hu X, Yu S, Liu Y, Xu Y, Huang X, Liu J, Yin B, Fan M, Peng X, Qiang B, et al. Nectin-like molecule 1 is a protein 4.1N associated protein and recruits protein 4.1N from cytoplasm to the plasma membrane. *Biochim Biophys Acta* 2005;1669:142–54.
26. Nickerson ML, Jaeger E, Shi Y, Durocher JA, Mahurkar S, Zaridze D, Matveev V, Janout V, Kollarova H, Bencko V, Navratilova M, Szeszenia-Dabrowska N, et al. Improved identification of von Hippel-Lindau gene alterations in clear cell renal tumors. *Clin Cancer Res* 2008;14: 4726–34.
27. Dall'Oglio MF, Antunes AA, Sarkis AS, Crippa A, Leite KR, Lucon AM, Srougi M. Microvascular tumour invasion in renal cell carcinoma: the most important prognostic factor. *BJ U Int* 2007;100:552–5.
28. Strewler GJ, Wronski TJ, Halloran BP, Miller SC, Leung SC, Williams RD, Nissenson RA. Pathogenesis of hypercalcemia in nude mice bearing a human renal carcinoma. *Endocrinology* 1986;119:303–10.
29. Dreijerink K, Braga E, Kuzmin I, Geil L, Duh FM, Angeloni D, Zbar B, Lerman MI, Stanbridge EJ, Minna JD, Protopopov A, Li J, et al. The candidate tumor suppressor gene, RASSF1A, from human chromosome 3p21.3 is involved in kidney tumorigenesis. *Proc Natl Acad Sci USA* 2001;98:7504–9.
30. Morrissey C, Martinez A, Zatyka M, Agathanggelou A, Honorio S, Astuti D, Morgan NV, Moch H, Richards FM, Kishida T, Yao M, Schraml P, et al. Epigenetic inactivation of the RASSF1A 3p21.3 tumor suppressor gene in both clear cell and papillary renal cell carcinoma. *Cancer Res* 2001;61:7277–81.
31. Dulaimi E, Caceres II, Uzzo RG, Al-Saleem T, Greenberg RE, Polascik TJ, Babb JS, Grizzle WE, Cairns P. Promoter hypermethylation profile of kidney cancer. *Clin Cancer Res* 2004;10:3972–9.
32. Murakami Y. Involvement of a cell adhesion molecule, TSLC1/IGSF4, in human oncogenesis. *Cancer Sci* 2005;96: 543–52.
33. Curto M, Cole BK, Lallemand D, Liu CH, McClatchey AI. Contact-dependent inhibition of EGFR signaling by Nf2/Merlin. *J Cell Biol* 2007;177:893–903.
34. Kunitz A, Wolter M, van den Boom J, Felsberg J, Tews B, Hahn M, Benner A, Sabel M, Lichter P, Reifenberger G, von Deimling A, Hartmann C. DNA hypermethylation and aberrant expression of the EMP3 gene at 19q13.3 in human gliomas. *Brain Pathol* 2007;17:363–70.
35. Tews B, Felsberg J, Hartmann C, Kunitz A, Hahn M, Toedt G, Neben K, Hummerich L, von Deimling A, Reifenberger G, Lichter P. Identification of novel oligodendroglioma-associated candidate tumor suppressor genes in 1p36 and 19q13 using microarray-based expression profiling. *Int J Cancer* 2006;119: 792–800.
36. Morris ZS, McClatchey A. Aberrant epithelial morphology and persistent epidermal growth factor receptor signaling in a mouse model of renal carcinoma. *Proc Natl Acad Sci USA* 2009;106:9767–72.
37. Sun CX, Robb VA, Gutmann DH. Protein 4.1 tumor suppressors: getting a FERM grip on growth regulation. *J Cell Sci* 2002; 115:3991–4000.
38. Kawano S, Ikeda W, Kishimoto M, Ogita H, Takai Y. Silencing of ErbB3/ErbB2 signaling by immunoglobulin-like Necl-2. *J Biol Chem* 2009;284:23793–805.
39. Doherty P, Walsh FS. CAM-FGF receptor interactions: a model for axonal growth. *Mol Cell Neurosci* 1996;8:99–111.
40. Surace EI, Lusis E, Murakami Y, Scheithauer BW, Perry A, Gutmann DH. Loss of tumor suppressor in lung cancer-1 (TSLC1) expression in meningioma correlates with increased malignancy grade and reduced patient survival. *J Neuropathol Exp Neurol* 2004;63:1015–27.

uicc
global cancer control

IJC
International Journal of Cancer

Genome structure-based screening identified epigenetically silenced microRNA associated with invasiveness in non-small-cell lung cancer

Kousuke Watanabe[1]*, Noriko Emoto[1]*, Emi Hamano[1], Mitsuhiro Sunohara[1], Masanori Kawakami[1], Hidenori Kage[1], Kentaro Kitano[2], Jun Nakajima[2], Akiteru Goto[3], Masashi Fukayama[3], Takahide Nagase[1], Yutaka Yatomi[4], Nobuya Ohishi[1] and Daiya Takai[4]

[1] Department of Respiratory Medicine, The University of Tokyo Hospital, Hongo, Bunkyo-ku, Tokyo, Japan
[2] Department of Cardiothoracic Surgery, The University of Tokyo Hospital, Hongo, Bunkyo-ku, Tokyo, Japan
[3] Department of Pathology, The University of Tokyo Hospital, Hongo, Bunkyo-ku, Tokyo, Japan
[4] Department of Clinical Laboratory, The University of Tokyo Hospital, Hongo, Bunkyo-ku, Tokyo, Japan

MicroRNA (miRNA) expression is frequently altered in human cancers. To search for epigenetically silenced miRNAs in non-small-cell lung cancer (NSCLC), we mapped human miRNAs on autosomal chromosomes and selected 55 miRNAs *in silico*. We treated six NSCLC cell lines with the DNA methylation inhibitor 5-aza-2′-deoxycytidine (5-aza-CdR) and determined the expressions of the 55 miRNAs. Fourteen miRNAs were decreased in the cancer cell lines and were induced after 5-aza-CdR treatment. After a detailed DNA methylation analysis, we found that mir-34b and mir-126 were silenced by DNA methylation. Mir-34b was silenced by the DNA methylation of its own promoter, whereas mir-126 was silenced by the DNA methylation of its host gene, *EGFL7*. A chromatin immunoprecipitation assay revealed H3K9me2 and H3K9me3 in mir-34b and *EGFL7*, and H3K27me3 in *EGFL7*. The overexpression of mir-34b and mir-126 decreased the expression of c-Met and Crk, respectively. The 5-aza-CdR treatment of lung cancer cell line resulted in increased mir-34b expression and decreased c-Met protein. We next analyzed the DNA methylation status of these miRNAs using 99 primary NSCLCs. Mir-34b and mir-126 were methylated in 41 and 7% of all the cases, respectively. The DNA methylation of mir-34b was not associated with c-Met expression determined by immunohistochemistry, but both mir-34b methylation ($p = 0.007$) and c-Met expression ($p = 0.005$) were significantly associated with lymphatic invasion in a multivariate analysis. The DNA methylation of mir-34b can be used as a biomarker for an invasive phenotype of lung cancer.

Cancer Genetics

MicroRNAs (miRNAs) are broadly conserved small non-coding RNA that regulate gene expression by binding to the 3′UTR of target mRNAs in a complementary manner.[1] Through the posttranscriptional regulation of many target genes, miRNAs are involved in many biological processes, such as development and human carcinogenesis. MicroRNA expression is altered in human cancers, and some miRNAs have oncogenic or tumor suppressive functions in human malignancies, including lung cancer.[2–5]

Key words: microRNA, DNA methylation, lung cancer
Additional Supporting Information may be found in the online version of this article.
*K.W. and N.E. contributed equally to the work.
Grant sponsor: Smoking Research Foundations, Takeda Science Foundation and KAKENHI; **Grant numbers:** 20659129, 22790749
DOI: 10.1002/ijc.26254
History: Received 7 Feb 2011; Accepted 1 Jun 2011; Online 23 Jun 2011
Correspondence to: Daiya Takai, M.D., PhD., Department of Clinical Laboratory, The University of Tokyo Hospital, 7-3-1, Hongo, Bunkyo-ku, Tokyo 113-8655, Japan, Tel.: +81-3-3815-5411 (extension 37725), Fax: +81 3 5689 0495, E-mail: dtakai-ind@umin.ac.jp

Chromosomal deletions or amplifications are important mechanisms of miRNA expression change in cancers. For example, mir-15 and mir-16 are frequently deleted and downregulated in chronic lymphocytic leukemia.[2] The mir-17-92 miRNA cluster is amplified and overexpressed in B-cell lymphoma[6] and lung cancer.[4] However, the precise mechanisms responsible for changes in miRNA expression in cancer remain largely unknown.

DNA methylation plays an important role in inactivating tumor suppressor genes in many types of human cancers.[7,8] Recently, DNA methylation in cancerous tissue has been shown to cause the silencing of miRNAs located in the vicinity of CpG islands.[9,10] As the epigenetic silencing of tumor suppressor genes is a common event in lung carcinogenesis[11–14] and miRNA expression is altered in lung cancer,[5] we decided to search for epigenetically silenced miRNAs in lung cancer.

In our study, we selected 55 candidate miRNAs *in silico* based on the genome structure and treated six non-small-cell lung cancer (NSCLC) cell lines with the DNA methylation inhibitor 5-aza-2′-deoxycytidine (5-aza-CdR). Among the suppressed miRNAs whose expressions were induced by 5-aza-CdR, we found that mir-34b and mir-126 were silenced

by DNA methylation. Mir-126 was silenced by the DNA methylation of its host gene, *EGFL7*. We then analyzed the histone modifications and the suppression of target genes by the overexpression of the miRNAs. We also determined the DNA methylation status of 99 primary NSCLCs and found that miRNA methylation was associated with histological invasiveness.

Material and Methods

Cell lines and 5-aza-CdR treatment

H1755, H2347, H1650, H1975, Calu-1, A549 and HEK293t were obtained from the American Type Culture Collection. LC1sq was obtained from the Health Science Research Resources Bank (Osaka, Japan). Normal human bronchial epithelial cell (NHBE) was obtained from Lonza (Basel, Switzerland). These cell lines were cultured according to each manufacturer's protocol. Genomic DNA was extracted using the standard proteinase K/phenol method,[15] and the total RNA was isolated using RNAiso (Takara, Shiga, Japan).

Six NSCLC cell lines (H1755, H2347, H1650, H1975, LC1sq and Calu-1) were treated with 5-aza-CdR (Sigma-Aldrich, St. Louis, MO) on Day 1 and Day 3 for 24 hr each time (3 μM for H2347, H1650 and H1975; 5 μM for H1755, LC1sq and Calu-1). Total RNA extraction and chromatin immunoprecipitation (ChIP) analysis were performed on Day 6.

Primary NSCLC samples

We analyzed 99 primary NSCLCs from 97 histologically confirmed NSCLC patients who had undergone surgical resection at the University of Tokyo Hospital. The two patients had double primary NSCLCs, *i.e.* they had two tumors showing different pathological characteristics. To determine the miRNA expression levels in a normal control, we used normal counterpart lung tissue of each patient and also normal lung tissue from a patient with sclerosing hemangioma who underwent surgical resection at the University of Tokyo Hospital. Informed consent was obtained from all the patients, and the study was approved by the Institutional Review Board. Genomic DNA, and the total RNA were isolated as described above.

MicroRNA expression analysis

The miRNA expression levels were analyzed using quantitative reverse transcription PCR (RT-PCR) using a TaqMan microRNA assay (Applied Biosystems, Foster City, CA), in accordance with the manufacturer's instructions. U6 small nuclear RNA (RNU6B) was used as an internal control. Detailed information regarding the 55 candidate miRNAs is available in Supporting Information Table 1.

Host gene expression analysis

The total RNA was reverse transcribed with Superscript III (Invitrogen, Carlsbad, CA), and the SYBR green RT-PCR was performed using Realtime PCR Master Mix (Toyobo, Osaka, Japan). Human Spleen Total RNA (Ambion, Austin, TX) was used as a positive control for the RT-PCR of the *EGFL7* long transcript. The beta-actin gene was used as an internal control. The PCR conditions and the primer sequences are shown in Supporting Information Table 2.

DNA methylation studies

A quantitative *Hpa*II PCR assay[16] was performed to measure the methylation levels of the six cancer cell lines and NHBE. Genomic DNA was digested with *Eco*RI (New England Biolabs, Ipswich, MA) and purified using phenol/chloroform extraction; 500 ng of *Eco*RI-digested DNA were then digested with *Hpa*II or *Msp*I (New England Biolabs). The percentage of DNA that was not digested by *Hpa*II was determined using real-time PCR with THUNDERBIRD SYBR qPCR Mix (Toyobo). *Msp*I was used to confirm that the *Hpa*II-digestion was blocked by DNA methylation, and not by a genetic change.

For the bisulfite sequencing, methylation-specific PCR (MSP) and combined bisulfite restriction analysis (COBRA), 500 ng of DNA was treated with sodium bisulfite according to a previously described protocol.[11] Bisulfite PCR and MSP were performed using Amplitaq Gold 360 Master Mix (Applied Biosystems). To ensure that an equal amount of DNA was used as a template, the genomic DNA of each clinical tumor sample was digested with *Hind*III (New England Biolabs), purified using phenol/chloroform extraction and quantified using a spectrophotometer before the bisulfite conversion reaction. Fifty nanograms of bisulfite-converted DNA was used as a template for the MSP, and the methylation status was determined using agarose gel electrophoresis after 35 cycles of amplification. For COBRA, the bisulfite PCR products were treated using ExoSAP-IT (US Biochemical, Cleveland, OH), as previously described,[17] digested using *Bst*UI or *Taq*I (New England Biolabs) and visualized using agarose gel electrophoresis.

The PCR conditions and the primer sequences are shown in Supporting Information Table 2.

Chromatin immunoprecipitation assay

The ChIP analysis was performed as previously described.[18] Briefly, cells were crosslinked with 1% formaldehyde followed by sonication using a BIORUPTOR (UCD-200TM; COSMO BIO, Tokyo, Japan). The sheared chromatin was then immunoprecipitated using OneDay ChIP Kit (Diagenode, Philadelphia, PA), and the immunoprecipitated DNA was quantified using real-time PCR with THUNDERBIRD SYBR qPCR Mix (Toyobo). The antibodies used were histone H3 (tri methyl K4) antibody (ab1012; abcam, Cambridge, MA), histone H3 (di methyl K9) antibody (ab1220; abcam), histone H3 (tri methyl K9) antibody (ab8898; abcam), histone H3 (tri methyl K27) antibody (ab6002; abcam) and the negative control IgG included in the kit. The HOXA9 gene was used as a positive control for the H3K27me3 antibody, as previously

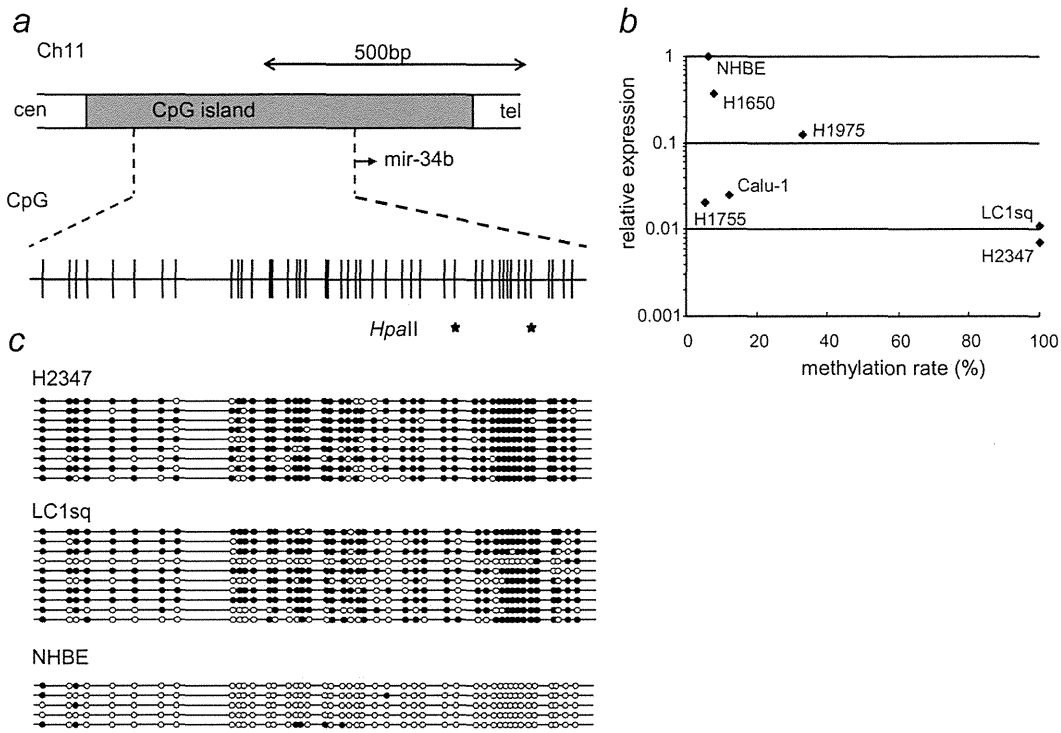

Figure 1. Epigenetic silencing of mir-34b. (*a*) Structure of mir-34b genomic locus. Mir-34b is located within a CpG island. The 5′ CpG sites and *Hpa*II sites for the DNA methylation analysis are also shown. (*b*) DNA methylation and mir-34b expression in six NSCLC cell lines and NHBE. The horizontal axis represents the DNA methylation rate determined using *Hpa*II PCR. The vertical axis represents the mir-34b expression relative to NHBE. We confirmed that more than 99% of the DNA was digested with *Msp*I in all the cell lines (data not shown), meaning that *Hpa*II digestion is blocked by DNA methylation. (*c*) Bisulfite sequencing. The open and filled circles represent unmethylated and methylated CpG sites, respectively.

described.[19,20] The PCR conditions and the primer sequences are shown in Supporting Information Table 2.

MicroRNA overexpression

The miRNA expression vector was constructed using a previously described pol III-dependent expression system.[21] The construction process is shown in Supporting Information Figure 1. Human U6 promoter containing a *Bsp*MI site was amplified using PCR with the primers U6pro-forward and U6pro-reverse-BspMI from the previously described plasmid U6pro/tetO/DNMT1,[21] then ligated into a TA cloning vector, pGEM-T Easy (Promega, Madison, WI). This plasmid was digested with *Bsp*MI (New England Biolabs), followed by the ligation of oligonucleotides (a mixture of two DNA oligomers, Oligo34bF and Oligo34bR or Oligo126F and Oligo126R) to form U6pro/mir-34b and U6pro/mir-126, respectively. A mir-126 expression cassette was triplicated to increase the expression of mature miRNA. The mir-126 expression cassette was amplified using PCR with the primers 126-forward-PstI and 126-reverse-SacI or 126-forward-SphI and 126-reverse-NcoI from U6pro/mir126, ligated into pGEM-T Easy and subcloned into the *Pst*I-*Sac*I site and *Sph*I-*Nco*I site of U6pro/mir-126. The resulting plasmid contained three miRNA expression cassettes (U6pro/mir-126*3). The mir-34b expression cassette was inverted by digestion with *Not*I (New England Biolabs). A hygromycin resistance cassette was then subcloned into the *Apa*I site from the previously described plasmid U6pro/tetO/DNMT1/hygro[21] to form U6pro/mir-34b/hygro, U6pro/mir-126*3/hygro/A and U6pro/mir-126*3/hygro/B. As a negative control, we used U6pro/Blank/hygro, which contained five Ts after the U6 promoter. The primer sequences are shown in Supporting Information Table 2.

Target gene analysis

The miRNA expression vectors and the control vector were transfected into A549 and HEK293t cells using Lipofectamine LTX reagent (Invitrogen), followed by hygromycin selection. After selection, the total protein was extracted using Radioimmunoprecipitation Assay (RIPA) buffer (phosphate buffered saline, 1% NP-40, 0.5% sodium deoxycholate, 0.1% sodium dodecyl sulfate) containing Complete Mini protease inhibitor (Roche, Basel, Switzerland), and the total RNA was isolated as described above. For the western blot analysis, 20 μg of total protein was loaded onto a 5–20% gradient

polyacrylamide gel (Wako, Osaka, Japan), electrophoresed in Tris-glycine-SDS running buffer, transferred to Hybond-P (GE Healthcare, Buckinghamshire, UK) and blotted with antibodies using the SNAP id system (Millipore, Billerica, MA). The antibodies used were c-Met antibody (1:60 dilution, sc-10; Santa Cruz Biotechnology, Santa Cruz, CA), Crk

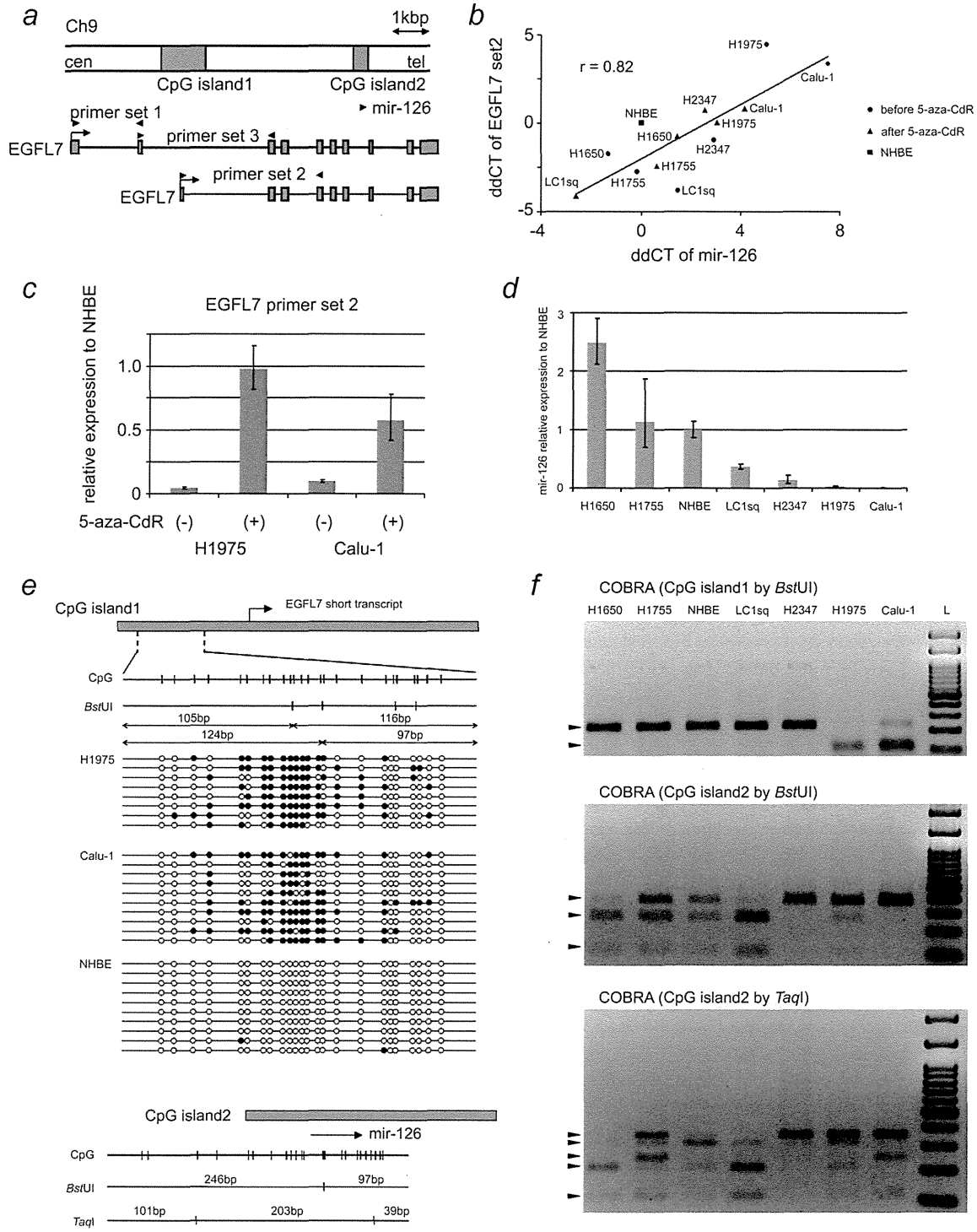

Figure 2.

II antibody (1:60 dilution, sc-9004; Santa Cruz Biotechnology), beta-actin antibody (1:3000 dilution, A5441; Sigma-Aldrich), anti-rabbit-IgG-horseradish peroxidase (HRP) antibody (1:1000 dilution for c-Met and Crk II, sc-2030; Santa Cruz Biotechnology) and anti-mouse-IgG-HRP antibody (1:2000 dilution for beta-actin, sc-2005; Santa Cruz Biotechnology). The proteins were detected using ECL plus solution (GE Healthcare) for c-Met and Crk II and ECL solution (GE Healthcare) for beta-actin. RT-PCR for c-Met and Crk was performed using THUNDERBIRD SYBR qPCR Mix (Toyobo). The PCR conditions and the primer sequences are shown in Supporting Information Table 2.

Immunohistochemistry for c-Met

A tissue microarray was constructed from formalin-fixed, paraffin-embedded tissue blocks. Immunohistochemistry was performed using antibodies against c-Met (1:100 dilution, SP44; Ventana Medical Systems, Tucson, AZ) using a Ventana Benchmark XT autostainer (Ventana Medical Systems). All the samples were evaluated by a pathologist (A.G.) who had no knowledge of any other data and were scored as previously described[22]: 0, complete absence of staining or only focal weak staining; 1, weak to moderate staining in less than 40% of the cancer cells; 2, weak to moderate staining in at least 40% of the cancer cells; and 3, strong staining in at least 10% of the cancer cells among the specimens with weak to moderate staining in at least 40% of the cancer cells. The cases were then divided into two groups: either c-Met negative (0, 1 or 2) or c-Met positive (3).

Statistical analysis

The relation between miRNA methylation, c-Met expression and clinicopathological characteristics were analyzed using chi-square test or Fisher's exact test. A logistic regression analysis was used to analyze independent factors associated with invasive phenotype. The analysis was performed using Dr.SPSS II (SPSS, Chicago, IL).

Results

Selection process of epigenetically silenced miRNAs

When our research started, the quantitative RT-PCR system using TaqMan microRNA assay (Applied Biosystems) was available for 687 miRNAs. We mapped these miRNAs on autosomal chromosomes and selected *in silico* 55 miRNAs that met one of the following criteria: (*i*) miRNAs within CpG islands, (*ii*) miRNAs within 1 kbp downstream of CpG islands and (*iii*) miRNAs within gene introns whose host promoters have CpG islands (Supporting Information Fig. 2 and Supporting Information Table 1).

After *in silico* selection, we treated six NSCLC cell lines (H1755, H2347, H1650, H1975, LC1sq and Calu-1) with 5-aza-CdR, and the expressions of the 55 miRNAs were determined (Supporting Information Fig. 3*a*). H1755 and H2347 were adenocarcinoma cell lines without epidermal growth factor receptor (EGFR) mutation; H1650 and H1975 were adenocarcinoma cell lines with EGFR mutation and LC1sq and Calu-1 were squamous cell carcinoma cell lines. The expression levels of 14 miRNAs (mir-375, mir-196b, mir-126, mir-34b, mir-127, mir-203, mir-148a, mir-181c, mir-30e, mir-449a, mir-340, mir-486, mir-483 and mir-139) were less than 25% of that in normal lung tissue and increased by more than 4-fold after 5-aza-CdR treatment. We then measured the expressions of these 14 miRNAs in 15 primary NSCLCs (Supporting Information Fig. 3*b*). Seven frequently suppressed miRNAs (mir-126, mir-34b, mir-203, mir-30e, mir-449a, mir-486 and mir-139) were selected as candidates for further analysis (Supporting Information Fig. 2).

Epigenetic silencing of mir-34b

Among the seven candidate miRNAs, three (mir-126, mir-34b and mir-203) were located within CpG islands. Mir-34b is frequently methylated in colorectal cancer,[23] and we used *HpaII* PCR to measure the level of DNA methylation of mir-34b in the six NSCLC cell lines and NHBE cells. These cell lines showed various levels of DNA methylation (Fig. 1*b*), and mir-34b was completely methylated in the two most suppressed cell lines, H2347 and LC1sq (Figs. 1*b* and 1*c*). The treatment of these two cell lines with 5-aza-CdR resulted in an increase in mir-34b expression (Supporting Information Fig. 3*a*). These results show that mir-34b expression is regulated by DNA methylation in NSCLC. Mir-203 is also located within a CpG island, but only a low level of DNA methylation was detected using bisulfite sequencing (data not shown).

Figure 2. Epigenetic silencing of mir-126. (*a*) Structure of *EGFL7* and mi-126 genomic locus. Mir-126 is located within a CpG island and also within the intron of *EGFL7*. The locations of the primers used for the RT-PCR of *EGFL7* are also shown. (*b*) Correlation between mir-126 expression and *EGFL7* expression before (circles) and after (triangles) 5-aza-CdR treatment. The horizontal axis represents the ddCt value of mir-126 relative to NHBE. The vertical axis represents the ddCt value of *EGFL7* relative to NHBE. The linear regression line and the Pearson's correlation coefficient (*r*) are indicated. (*c*) Induction of *EGFL7* by 5-aza-CdR treatment in H1975 and Calu-1. Experiments were duplicated, and the error bars indicate the standard deviation (SD). (*d*) Mir-126 expression in six cancer cell lines (before 5-aza-CdR treatment) and NHBE. Experiments were triplicated, and the error bars indicate the SD. (*e*) Bisulfite sequencing of CpG island 1 in H1975, Calu-1, and NHBE. The CpG sites and *Bst*UI sites used for COBRA are also indicated. Open and filled circles represent unmethylated and methylated CpG sites, respectively. The CpG sites and *Bst*UI and *Taq*I sites for COBRA within CpG island 2 are shown at the bottom. (*f*) COBRA of CpG island 1 and CpG island 2 in six cancer cell lines and NHBE. The lanes are arranged in the order of mir-126 expression from left (high expression) to right (low expression). Arrowheads indicate undigested and digested DNA fragments (L, 100-bp DNA ladder).

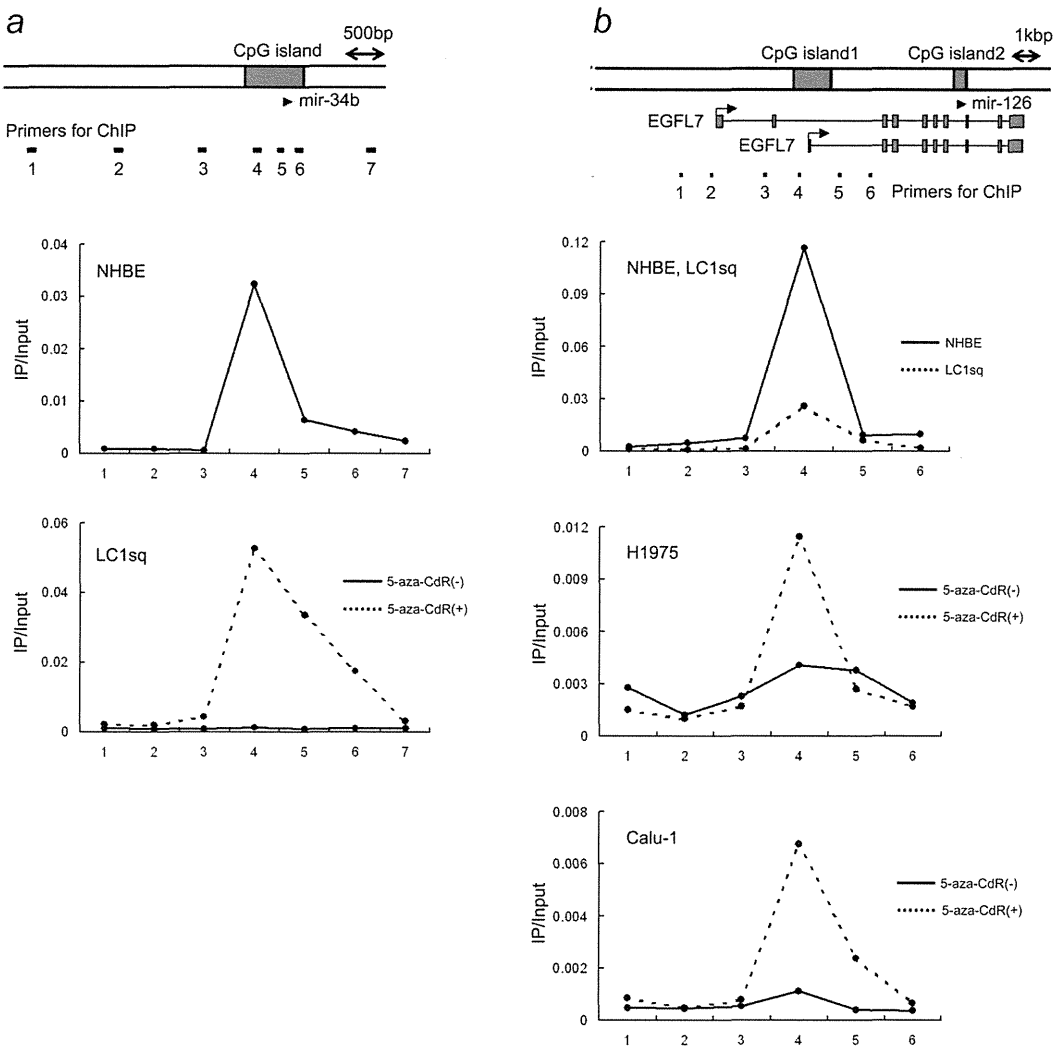

Figure 3. H3K4 trimethylation of mir-34b and mir-126. (*a*) Mapping of H3K4me3 at the mir-34b locus. The locations of the PCR primers used for ChIP are indicated. The experiments were duplicated, and the results are shown as the ratios of immunoprecipitated (IP) DNA to input DNA. (*b*) Mapping of H3K4me3 at *EGFL7* and the mir-126 locus; Otherwise as shown in Figure 3*a*.

Epigenetic silencing of mir-126 through the methylation of its host gene, EGFL7

Mir-126 is located within a CpG island and also within the intron of *EGFL7* (Fig. 2*a*). According to the UCSC Genome Bioinformatics Site (http://genome.ucsc.edu), *EGFL7* has several transcriptional variants, and one short transcript has another CpG island at its 5′ end (Fig. 2*a*).

The long *EGFL7* transcript (primer set 1, shown in Fig. 2*a*) was detected in the spleen but not in NHBE or the six NSCLC cell lines with or without 5-aza-CdR treatment (data not shown). In contrast, the short *EGFL7* transcript (primer set 2, shown in Fig. 2*a*) was detected in NHBE and the six NSCLC cell lines, and the expression of mir-126 and the short *EGFL7* transcript were strongly correlated (Pearson's correlation coefficient = 0.82, $p = 0.00048$; Fig. 2*b*). The expression of mir-126 and the *EGFL7* short transcript was significantly suppressed in H1975 and Calu-1 (Figs. 2*b*–2*d*). The 5-aza-CdR treatment of H1975 and Calu-1 restored the expression of mir-126 and the *EGFL7* short transcript (Figs. 2*b* and 2*c*), but the long *EGFL7* transcript (primer set 1 or 3) was not detected even after the 5-aza-CdR treatment of these two cell lines.

The 5′ CpG island of the *EGFL7* short transcript was heavily methylated in H1975 and Calu-1 but not in NHBE (Fig. 2*e*). To analyze the relation of the CpG island methylation status and miRNA expression, we performed a combined bisulfite restriction analysis (COBRA)[24] of the two CpG islands (CpG island 1 and CpG island 2, shown in Fig. 2*a*).

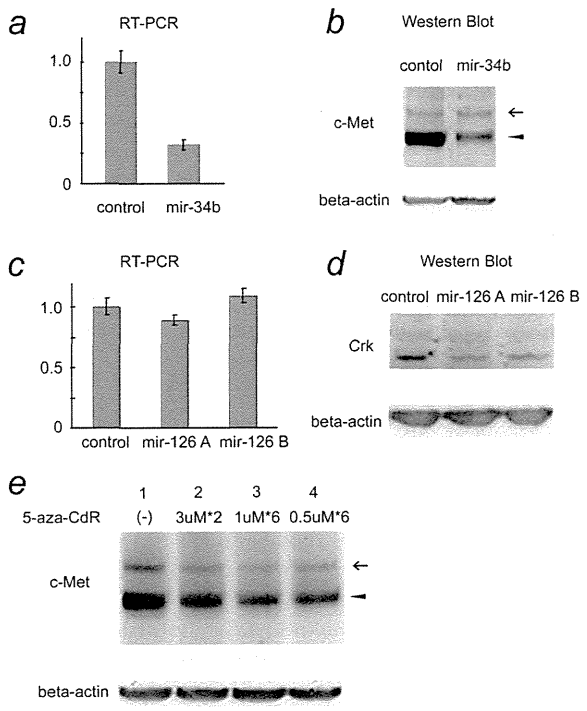

Figure 4. Analysis of miRNA targets. (*a*) RT-PCR of c-Met after the introduction of mir-34b into A549 cells. The vertical axis indicates the relative expression compared to that of the control vector. Experiments were duplicated, and the error bars indicate the SD. (*b*) Western blot of c-Met after the introduction of mir-34b into A549 cells. Both the c-Met precursor (arrow) and the c-Met beta subunit (arrowhead) are visible. (*c*) RT-PCR of Crk after the introduction of mir-126 into HEK293t cells. The vertical axis indicates the relative expression compared to that of the control vector. Experiments were triplicated, and the error bars indicate the SD. (*d*) Western blot of Crk after the introduction of mir-126 into HEK293t cells. Both mir-126A and mir-126B are miRNA expression vectors, but they have hygromycin resistance cassettes in different directions (Refer to Supporting Information Fig. 1). (*e*) Reduced c-Met protein after 5-aza-CdR treatment in H2347 cells. H2347 cells were treated with various concentrations of 5-aza-CdR (Lane 1, no treatment; Lane 2, 3 μM for 24 hr on Day 1 and Day 3, total protein was isolated on Day 6; Lane 3, 1 μM for six consecutive days, medium was changed every day, total protein was isolated on Day 7 and Lane 4, 0.5 μM for six consecutive days, medium was changed every day, total protein was isolated on Day 7). Both the c-Met precursor (arrow) and the c-Met beta subunit (arrowhead) are visible, similar to Figure 4*b*.

The DNA methylation of CpG island 1 was associated with a decrease in mir-126 expression. In contrast, the DNA methylation of CpG island 2 was not related to the expression of mir-126 (Fig. 2*f*). These results show that mir-126 is epigenetically silenced by the DNA methylation of its host gene, *EGFL7*.

We also analyzed the expression of intronic miRNAs and their host genes for the four remaining candidate miRNAs (mir-30e, mir-449a, mir-486 and mir-139; Supporting Information Fig. 4). The expressions of mir-139 and mir-449a were correlated with the expressions of their host genes, PED2A and CDC20B, respectively. However, the CpG islands of these host genes had only a low level of methylation in our NSCLC cell lines (data not shown).

Chromatin immunoprecipitation assay

To further analyze the regulation of miRNA expression, we examined the histone modifications of mir-34b and mir-126 using a ChIP assay. We observed the enrichment of H3K4me3 in the 5′ region of mir-34b in NHBE, but not in LC1sq (Fig. 3*a*). The H3K4me3 peak was restored in LC1sq after 5-aza-CdR treatment (Fig. 3*a*). Mir-34b was enriched with H3K9 methylation (H3K9me2 and H3K9me3) in LC1sq and, contrary to our expectations, also in NHBE (Supporting Information Fig. 5*b*). Although we cannot rule out the possibility of the nonspecific binding of the H3K9me2 and H3K9me3 antibodies, H3K9 methylation can occur without DNA methylation.[25] In fact, the relative mir-34b expression level in NHBE, compared to that in normal lung tissue, was 0.11 (0.10–0.13, mean ± SD), and the H3K9 methylation of NHBE may explain this suppression.

For the analysis of mir-126, we used two cell lines without CpG island methylation (NHBE and LC1sq) and two cell lines with heavily methylated CpG islands (H1975 and Calu-1). We detected the H3K4me3 peak in NHBE and LC1sq (Fig. 3*b*). This peak was very small in H1975 and Calu-1 and was induced after 5-aza-CdR treatment in both cell lines (Fig. 3*b*). The location of the H3K4me3 peak (primer 4, shown in Fig. 3*b*) was the same as the region of DNA methylation observed in H1975 and Calu-1 (shown in Fig. 2*e*). These results indicate that the DNA methylation near the transcriptional start site regulates *EGFL7* and mir-126 expression.

Unlike mir-34b, the *EGFL7* locus was enriched not only with H3K9 methylation but also with H3K27me3 (Supporting Information Fig. 5*c*). H3K27me3 was especially enriched in H1975, suggesting that both DNA methylation and H3K27me3 contribute to the epigenetic silencing of mir-126.

Target gene analysis of mir-34b and mir-126

To identify the target genes of mir-34b and mir-126, we used a database for the prediction of miRNA targets (Target Scan Human, http://targetscan.org).[26] Among the numerous predicted targets of mir-34b, we selected c-Met because c-Met has an oncogenic function in many human malignancies.[27] The overexpression of mir-34b using a U6 promoter-based expression vector[21] in A549 resulted in the decreased expression of c-Met at both the mRNA and protein levels (Figs. 4*a* and 4*b*). Mir-34b was completely methylated in H2347 (Figs. 1*b* and 1*c*), and the treatment of this cell line with 5-aza-CdR decreased the c-Met protein level (Fig. 4*e*).

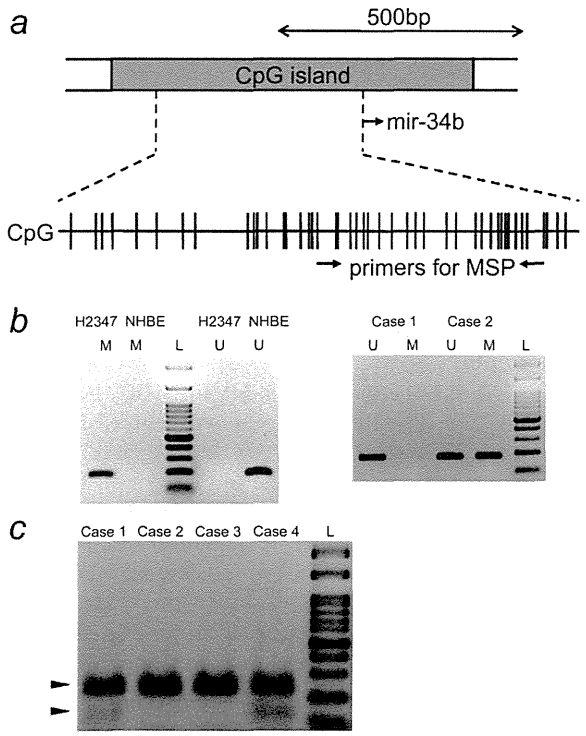

Figure 5. Methylation analysis of clinical tumor samples. Structure of mir-34b locus. (*a*) The CpG sites and the locations of the MSP primers are shown. (*b*) MSP analysis of mir-34b. H2347 and NHBE were used for the methylated and unmethylated controls. The bands in the "M" lanes are PCR products obtained using methylation-specific primers. The bands in the "U" lanes are PCR products obtained using unmethylated-specific primers. Mir-34b was methylated in case 2 but not in case 1. (*c*) COBRA of mir-126. Arrowheads indicate undigested and digested DNA fragments. Mir-126 was methylated in cases 1 and 4 (L, 100-bp DNA ladder).

We selected Crk as the target of mir-126 because an increase in Crk expression is associated with an aggressive phenotype in lung adenocarcinoma.[28] In agreement with previous reports[29,30] the overexpression of mir-126 in HEK293t decreased the Crk protein level without a significant change in the mRNA level (Figs. 4*c* and 4*d*).

DNA methylation analysis of primary NSCLCs and pathological characteristics

We analyzed the DNA methylation status of the two miRNAs in 99 primary NSCLCs, including 80 cases of adenocarcinoma, 18 cases of squamous cell carcinoma and 1 case of both histological components. There were 41 cases with T1 disease (<30 mm in diameter) without lymph node metastasis, 14 cases with T1 disease with lymph node metastasis, 27 cases with T2 disease (more than 30 mm in diameter or pleural invasion) without lymph node metastasis and 17 cases with T2 disease with lymph node metastasis. The DNA methylation status of mir-34b was determined using MSP[31] (Figs. 5*a* and 5*b*). For mir-126, the DNA methylation status of the 5′ CpG island of *EGFL7* was determined using COBRA (Fig. 5*c*; same protocol as that used for COBRA of CpG island 1, shown in Figs. 2*e* and 2*f*). We attempted to design MSP primers for the methylation analysis of mir-126, but the region of DNA methylation was less than 100 bp (Fig. 2*e*), and we could not design appropriate primers in this region. PCR amplification was successful in 96 samples.

Mir-34b and mir-126 were methylated in 40 (41%) and 7 (7%) of 96 the samples, respectively. To analyze the impact of miRNA methylation on the expression of a target oncogene, we performed immunohistochemistry for c-Met in 89 cases (Supporting Information Fig. 6). However, no correlation was observed between the miRNA methylation status and the c-Met expression level [(b) in Table 1], meaning that other mechanisms, such as gene amplification, are important for determining the c-Met expression level.

In a univariate analysis, both mir-34b methylation (chi-square test, $p = 0.016$) and c-Met expression (Fisher's exact test, $p = 0.026$) were associated with lymphatic invasion [(b and c) in Table 1]. In a multivariate analysis (stepwise logistic regression analysis), both mir-34b methylation ($p = 0.007$, odds ratio = 5.4) and c-Met expression ($p = 0.005$, odds ratio = 6.4) were associated with lymphatic invasion, whereas other clinical variables (age, gender, smoking, histology and tumor size) were not associated with lymphatic invasion [(d) in Table 1]. Therefore, both mir-34b methylation and c-Met expression were independent risk factors for lymphatic invasion.

The mir-126 methylation tended to be more frequent in tumors with venous invasion [(b) in Table 1], but the difference was not statistically significant (Fisher's exact test, $p = 0.084$). The mir-126 methylation was not associated with venous invasion in a multivariate analysis (data not shown).

Discussion

In our study, we analyzed 55 candidate miRNAs of which two were silenced by DNA methylation. The silencing mechanisms of the two miRNAs were different. Mir-34b was silenced by the DNA methylation of its own promoter, whereas mir-126 was silenced by the DNA methylation of its host gene's promoter.

Our initial *in silico* selected miRNAs included nine miRNAs within 1 kbp downstream of CpG islands, but none of these miRNAs were silenced by DNA methylation. This result may be partly because the primary miRNA transcripts are sometimes transcribed from more than 1 kb upstream of mature miRNAs, such as mir-21 and mir-155.[32,33] Further research is required for the epigenetic regulation of miRNAs, especially those located more than 1 kb downstream of CpG islands or those located within introns and coregulated with their host genes.

The mir-34 family consists of three miRNAs (mir-34a, mir-34b and mir-34c) that are derived from two transcripts

Table 1. MiRNA methylation and clinicopathological characteristics

(a) Clinical backgrounds of 96 cases in which PCR amplification was successful	
	Number of cases (*n*)
Age	≥65 years, *n* = 51; <65 years, *n* = 45
Gender	Male, *n* = 59; female, *n* = 37
Smoking	Smoker, *n* = 63; nonsmoker, *n* = 33
Histology	Adenocarcinoma, *n* = 78; squamous cell carcinoma, *n* = 17; adenosquamous carcinoma, *n* = 1
Tumor size	T1, *n* = 53; T2, *n* = 43

(b) Correlation of miRNA methylation and pathological characteristics				
		Methylated (*n*)	Unmethylated (*n*)	*p* Values
mir-34b methylation and lymphatic invasion	Invasion (–)	25	47	
	Invasion (+)	15	9	0.016[1]
mir-34b methylation and venous invasion	Invasion (–)	22	36	
	Invasion (+)	18	20	0.35[1]
mir-126 methylation and lymphatic invasion	Invasion (–)	4	68	
	Invasion (+)	3	21	0.23[2]
mir-126 methylation and venous invasion	Invasion (–)	2	56	
	Invasion (+)	5	33	0.084[2]
mir-34b methylation and c-Met expression	c-Met (–)	31	39	
	c-Met (+)	5	14	0.15[1]

(c) Correlation of clinicopathological characteristics and lymphatic invasion				
	Invasions	Number of cases (*n*)		*p* Values
Age	(–)	≥65 years, *n* = 36	<65 years, *n* = 36	
	(+)	≥65 years, *n* = 15	<65 years, *n* = 9	0.28[1]
Gender	(–)	Male, *n* = 44	Female, *n* = 28	
	(+)	Male, *n* = 15	Female, *n* = 9	0.90[1]
Smoking	(–)	Smoker, *n* = 47	Nonsmoker, *n* = 25	
	(+)	Smoker, *n* = 16	Nonsmoker, *n* = 8	0.90[1]
Histology	(–)	Adenocarcinoma, *n* = 59	Squamous cell carcinoma, *n* = 13	
	(+)	Adenocarcinoma, *n* = 19	Squamous cell carcinoma, *n* = 4	0.60[2]
Tumor size	(–)	T1, *n* = 41	T2, *n* = 31	
	(+)	T1, *n* = 12	T2, *n* = 12	0.55[1]
c-Met expression	(–)	c-Met (+), *n* =11	c-Met (–), *n* = 58	
	(+)	c-Met (+), *n* = 8	c-Met (–), *n* = 12	0.026[2]

(d) Stepwise logistic regression analysis for risk factors of lymphatic invasion		
	Odds ratio (95 % confidential interval)	*p* Values
mir-34b methylation (methylated or unmethylated)	5.494 (1.585–19.047)	0.007
c-Met expression (positive or negative)	6.492 (1.738–24.256)	0.005

[1]Chi-square test. [2]Fisher's exact test.

(mir-34a on chromosome 1 and mir-34b/c on chromosome 11). Mir-34s have been shown to be direct targets of p53.[34–36] Interestingly, mir-34a is most highly expressed in the brain, whereas mir-34b/c is most highly expressed in the lung with a low expression in the brain and no expression in any other tissues,[36] suggesting that mir-34b/c plays an important role in the p53 tumor suppressive pathway, at least in lung tissue.

In our study, we showed the importance of DNA methylation in the regulation of mir-34b expression in lung cancer and the suppression of the c-Met oncogene by its overexpression. Among the numerous predicted targets of mir-34b, we selected c-Met for further analysis, because it is an important target of cancer therapy,[37] and its amplification has been reported to be a mechanism of acquired resistance to gefitinib therapy in NSCLC.[38] We observed increased mir-34b

expression and reduced c-Met protein after 5-aza-CdR treatment of H2347 cells. This does not necessarily mean that mir-34b reexpression was responsible for c-Met reduction, as 5-aza-CdR treatment induces many silenced genes. A recent study showed that treatment of the colon cancer cell line HCT116 with 5-aza-CdR induced an abnormal fusion transcript of LINE-1 and c-Met that did not code for a normal c-Met protein.[39] Further research is required to understand the molecular basis of epigenetic drug actions.

We also observed a strong association between mir-34b methylation and lymphatic invasion in clinical tumor samples, in agreement with a previous report that mir-34b methylation is correlated with metastasis in human cancers.[10] Migliore *et al.*[40] reported that mir-34s suppress c-Met and impair invasion in several cancer cell lines. In their study, c-Met overexpression rescued impaired cell invasion, and therefore, they concluded that mir-34s suppress invasion through the downregulation of c-Met *in vitro*. However, in our study, mir-34b methylation and c-Met expression were independent, and both of them were associated with lymphatic invasion. Our results suggest that the regulation of c-Met expression and tumor invasion is more complex *in vivo*. Although the pathological phenotype associated with mir-34b methylation was similar to that associated with c-Met overexpression, the loss of mir-34b probably does not induce c-Met overexpression directly in primary NSCLCs.

Mir-126 is a tumor suppressive miRNA, suppressing metastasis in breast cancer[41] and inhibiting invasion by targeting Crk in NSCLC.[29] Using bladder cancer cell lines, Saito reported that epigenetic therapy upregulates mir-126 and its host gene *EGFL7*, but DNA methylation was not detected in the *EGFL7* promoter region.[42] Here, we showed that mir-126 is silenced by the DNA methylation of its host gene, *EGFL7* in lung cancer. Many miRNAs are located within introns of protein coding genes, and intronic miRNAs are usually coordinately expressed with their host gene mRNAs.[43] Grady reported that mir-342 is epigenetically silenced by the DNA methylation of its host gene, Enah/Vasp-like (EVL) in colorectal cancer[44]; thus, mir-126 is the second miRNA silenced by the DNA methylation of its host gene.

We also showed that the *EGFL7* locus was enriched with H3K27me3, which is consistent with a previous report that polycomb-mediated H3K27me3 premarks genes for *de novo* DNA methylation in colon cancer.[20] In contrast, Kondo reported that H3K27me3 mediates gene silencing independent of DNA methylation in prostate cancer.[45] Although mir-126 expression was frequently suppressed in clinical tumor samples, the frequency and the degree of DNA methylation were low in our analysis using COBRA, and this discrepancy may be explained by H3K27me3.

In conclusion, genome structure-based screening was used to identify two epigenetically silenced tumor suppressive miRNAs. Our genome-structure based approach can be applied to identify epigenetically silenced miRNAs in other malignancies. The DNA methylation of mir-34b can be used as a biomarker for an invasive phenotype of lung cancer.

References

1. Bartel DP. MicroRNAs: genomics, biogenesis, mechanism, and function. *Cell* 2004;116:281–97.
2. Calin GA, Dumitru CD, Shimizu M, Bichi R, Zupo S, Noch E, Aldler H, Rattan S, Keating M, Rai K, Rassenti L, Kipps T, et al. Frequent deletions and down-regulation of micro- RNA genes miR15 and miR16 at 13q14 in chronic lymphocytic leukemia. *Proc Natl Acad Sci USA* 2002;99:15524–9.
3. Takamizawa J, Konishi H, Yanagisawa K, Tomida S, Osada H, Endoh H, Harano T, Yatabe Y, Nagino M, Nimura Y, Mitsudomi T, Takahashi T. Reduced expression of the let-7 microRNAs in human lung cancers in association with shortened postoperative survival. *Cancer Res* 2004;64:3753–6.
4. Hayashita Y, Osada H, Tatematsu Y, Yamada H, Yanagisawa K, Tomida S, Yatabe Y, Kawahara K, Sekido Y, Takahashi T. A polycistronic microRNA cluster, miR-17–92, is overexpressed in human lung cancers and enhances cell proliferation. *Cancer Res* 2005;65:9628–32.
5. Yanaihara N, Caplen N, Bowman E, Seike M, Kumamoto K, Yi M, Stephens RM, Okamoto A, Yokota J, Tanaka T, Calin GA, Liu CG, et al. Unique microRNA molecular profiles in lung cancer diagnosis and prognosis. *Cancer Cell* 2006;9: 189–98.
6. He L, Thomson JM, Hemann MT, Hernando-Monge E, Mu D, Goodson S, Powers S, Cordon-Cardo C, Lowe SW, Hannon GJ, Hammond SM. A microRNA polycistron as a potential human oncogene. *Nature* 2005;435:828–33.
7. Jones PA, Baylin SB. The fundamental role of epigenetic events in cancer. *Nat Rev Genet* 2002;3:415–28.
8. Herman JG, Baylin SB. Gene silencing in cancer in association with promoter hypermethylation. *N Engl J Med* 2003;349: 2042–54.
9. Saito Y, Liang G, Egger G, Friedman JM, Chuang JC, Coetzee GA, Jones PA. Specific activation of microRNA-127 with downregulation of the proto-oncogene BCL6 by chromatin-modifying drugs in human cancer cells. *Cancer Cell* 2006;9: 435–43.
10. Lujambio A, Calin GA, Villanueva A, Ropero S, Sanchez-Cespedes M, Blanco D, Montuenga LM, Rossi S, Nicoloso MS, Faller WJ, Gallagher WM, Eccles SA, et al. A microRNA DNA methylation signature for human cancer metastasis. *Proc Natl Acad Sci USA* 2008;105:13556–61.
11. Sano A, Kage H, Sugimoto K, Kitagawa H, Aki N, Goto A, Fukayama M, Nakajima J, Takamoto S, Nagase T, Yatomi Y, Ohishi N, et al. A second-generation profiling system for quantitative methylation analysis of multiple gene promoters: application to lung cancer. *Oncogene* 2007; 26:6518–25.
12. Kusakabe M, Kutomi T, Watanabe K, Emoto N, Aki N, Kage H, Hamano E, Kitagawa H, Nagase T, Sano A, Yoshida Y, Fukami T, et al. Identification of G0S2 as a gene frequently methylated in squamous lung cancer by combination of in silico and experimental approaches. *Int J Cancer* 2010;126:1895–902.
13. Brock MV, Hooker CM, Ota-Machida E, Han Y, Guo M, Ames S, Glockner S, Piantadosi S, Gabrielson E, Pridham G, Pelosky K, Belinsky SA, et al. DNA methylation markers and early recurrence in stage I lung cancer. *N Engl J Med* 2008; 358:1118–28.
14. Takai D, Yagi Y, Wakazono K, Ohishi N, Morita Y, Sugimura T, Ushijima T. Silencing of HTR1B and reduced expression of EDN1 in human lung

cancers, revealed by methylation-sensitive representational difference analysis. *Oncogene* 2001;20:7505–13.
15. Sambrook J, Russell DW. Molecular Cloning 3rd Editioned., vol. 1, chapter 6. New York:CSHL Press, 2001.
16. Singer-Sam J, LeBon JM, Tanguay RL, Riggs AD. A quantitative HpaII-PCR assay to measure methylation of DNA from a small number of cells. *Nucleic Acids Res* 1990;18:687.
17. Watanabe K, Emoto N, Sunohara M, Kawakami M, Kage H, Nagase T, Ohishi N, Takai D. Treatment of PCR products with exonuclease I and heat-labile alkaline phosphatase improves the visibility of combined bisulfite restriction analysis. *Biochem Biophys Res Commun* 2010;399: 422–4.
18. Kusakabe M, Watanabe K, Emoto N, Aki N, Kage H, Nagase T, Nakajima J, Yatomi Y, Ohishi N, Takai D. Impact of DNA demethylation of the G0S2 gene on the transcription of G0S2 in squamous lung cancer cell lines with or without nuclear receptor agonists. *Biochem Biophys Res Commun* 2009;390:1283–7.
19. Cao R, Zhang Y. SUZ12 is required for both the histone methyltransferase activity and the silencing function of the EED-EZH2 complex. *Mol Cell* 2004;15: 57–67.
20. Schlesinger Y, Straussman R, Keshet I, Farkash S, Hecht M, Zimmerman J, Eden E, Yakhini Z, Ben-Shushan E, Reubinoff BE, Bergman Y, Simon I, et al. Polycomb-mediated methylation on Lys27 of histone H3 pre-marks genes for de novo methylation in cancer. *Nat Genet* 2007;39: 232–6.
21. Matsukura S, Jones PA, Takai D. Establishment of conditional vectors for hairpin siRNA knockdowns. *Nucleic Acids Res* 2003;31:e77.
22. Nakamura Y, Niki T, Goto A, Morikawa T, Miyazawa K, Nakajima J, Fukayama M. c-Met activation in lung adenocarcinoma tissues: an immunohistochemical analysis. *Cancer Sci* 2007;98:1006–13.
23. Toyota M, Suzuki H, Sasaki Y, Maruyama R, Imai K, Shinomura Y, Tokino T. Epigenetic silencing of microRNA-34b/c and B-cell translocation gene 4 is associated with CpG island methylation in colorectal cancer. *Cancer Res* 2008;68: 4123–32.
24. Xiong Z, Laird PW. COBRA: a sensitive and quantitative DNA methylation assay. *Nucleic Acids Res* 1997;25:2532–4.
25. Bachman KE, Park BH, Rhee I, Rajagopalan H, Herman JG, Baylin SB, Kinzler KW, Vogelstein B. Histone modifications and silencing prior to DNA methylation of a tumor suppressor gene. *Cancer Cell* 2003;3:89–95.
26. Grimson A, Farh KK, Johnston WK, Garrett-Engele P, Lim LP, Bartel DP. MicroRNA targeting specificity in mammals: determinants beyond seed pairing. *Mol Cell* 2007;27:91–105.
27. Peruzzi B, Bottaro DP. Targeting the c-Met signaling pathway in cancer. *Clin Cancer Res* 2006;12:3657–60.
28. Miller CT, Chen G, Gharib TG, Wang H, Thomas DG, Misek DE, Giordano TJ, Yee J, Orringer MB, Hanash SM, Beer DG. Increased C-CRK proto-oncogene expression is associated with an aggressive phenotype in lung adenocarcinomas. *Oncogene* 2003;22:7950–7.
29. Crawford M, Brawner E, Batte K, Yu L, Hunter MG, Otterson GA, Nuovo G, Marsh CB, Nana-Sinkam SP. MicroRNA-126 inhibits invasion in non-small cell lung carcinoma cell lines. *Biochem Biophys Res Commun* 2008;373:607–12.
30. Li X, Shen Y, Ichikawa H, Antes T, Goldberg GS. Regulation of miRNA expression by Src and contact normalization: effects on nonanchored cell growth and migration. *Oncogene* 2009;28: 4272–83.
31. Herman JG, Graff JR, Myohanen S, Nelkin BD, Baylin SB. Methylation-specific PCR: a novel PCR assay for methylation status of CpG islands. *Proc Natl Acad Sci USA* 1996; 93:9821–6.
32. Cai X, Hagedorn CH, Cullen BR. Human microRNAs are processed from capped, polyadenylated transcripts that can also function as mRNAs. *RNA* 2004;10:1957–66.
33. Eis PS, Tam W, Sun L, Chadburn A, Li Z, Gomez MF, Lund E, Dahlberg JE. Accumulation of miR-155 and BIC RNA in human B cell lymphomas. *Proc Natl Acad Sci USA* 2005;102:3627–32.
34. Corney DC, Flesken-Nikitin A, Godwin AK, Wang W, Nikitin AY. MicroRNA-34b and MicroRNA-34c are targets of p53 and cooperate in control of cell proliferation and adhesion-independent growth. *Cancer Res* 2007;67:8433–8.
35. He L, He X, Lim LP, de Stanchina E, Xuan Z, Liang Y, Xue W, Zender L, Magnus J, Ridzon D, Jackson AL, Linsley PS, et al. A microRNA component of the p53 tumour suppressor network. *Nature* 2007;447: 1130–4.
36. Bommer GT, Gerin I, Feng Y, Kaczorowski AJ, Kuick R, Love RE, Zhai Y, Giordano TJ, Qin ZS, Moore BB, MacDougald OA, Cho KR, et al. p53-mediated activation of miRNA34 candidate tumor-suppressor genes. *Curr Biol* 2007;17:1298–307.
37. Eder JP, Vande Woude GF, Boerner SA, LoRusso PM. Novel therapeutic inhibitors of the c-Met signaling pathway in cancer. *Clin Cancer Res* 2009;15:2207–14.
38. Engelman JA, Zejnullahu K, Mitsudomi T, Song Y, Hyland C, Park JO, Lindeman N, Gale CM, Zhao X, Christensen J, Kosaka T, Holmes AJ, et al. MET amplification leads to gefitinib resistance in lung cancer by activating ERBB3 signaling. *Science* 2007;316:1039–43.
39. Weber B, Kimhi S, Howard G, Eden A, Lyko F. Demethylation of a LINE-1 antisense promoter in the cMet locus impairs Met signalling through induction of illegitimate transcription. *Oncogene* 2010;29:5775–84.
40. Migliore C, Petrelli A, Ghiso E, Corso S, Capparuccia L, Eramo A, Comoglio PM, Giordano S. MicroRNAs impair MET-mediated invasive growth. *Cancer Res* 2008;68:10128–36.
41. Tavazoie SF, Alarcon C, Oskarsson T, Padua D, Wang Q, Bos PD, Gerald WL, Massague J. Endogenous human microRNAs that suppress breast cancer metastasis. *Nature* 2008;451:147–52.
42. Saito Y, Friedman JM, Chihara Y, Egger G, Chuang JC, Liang G. Epigenetic therapy upregulates the tumor suppressor microRNA-126 and its host gene EGFL7 in human cancer cells. *Biochem Biophys Res Commun* 2009;379:726–31.
43. Baskerville S, Bartel DP. Microarray profiling of microRNAs reveals frequent coexpression with neighboring miRNAs and host genes. *RNA* 2005;11: 241–7.
44. Grady WM, Parkin RK, Mitchell PS, Lee JH, Kim YH, Tsuchiya KD, Washington MK, Paraskeva C, Willson JK, Kaz AM, Kroh EM, Allen A, et al. Epigenetic silencing of the intronic microRNA hsa-miR-342 and its host gene EVL in colorectal cancer. *Oncogene* 2008;27: 3880–8.
45. Kondo Y, Shen L, Cheng AS, Ahmed S, Boumber Y, Charo C, Yamochi T, Urano T, Furukawa K, Kwabi-Addo B, Gold DL, Sekido Y, et al. Gene silencing in cancer by histone H3 lysine 27 trimethylation independent of promoter DNA methylation. *Nat Genet* 2008;40:741–50.

Pulmonary Venous Invasion, Determined by Chest Computed Tomographic Scan, as a Potential Early Indicator of Zygomycosis Infection

A Case Series

Hiroshi Kitagawa, MD, PhD, Kousuke Watanabe, MD,* Hidenori Kage, MD, PhD,* Shinichi Inoh, MD,† Akiteru Goto, MD, PhD,‡ Masashi Fukayama, MD, PhD,‡ Takahide Nagase, MD, PhD,* Nobuya Ohishi, MD, PhD,* and Daiya Takai, MD, PhD§*

Abstract: Zygomycosis is a life-threatening fungal infection, and its successful treatment requires early diagnosis. To establish radiologic and clinical criteria for early diagnosis, we reviewed 3 postmortem cases with zygomycosis secondary to hematological diseases. In all cases, an irregular dilatation of pulmonary veins on computed tomography suggested venous invasion by fungal hyphae, which was confirmed at autopsy. In addition, serum samples tested negative for the Aspergillus galactomannan antigen in all cases. These distinguishing radiologic and clinical features may contribute to an earlier diagnosis; more radical treatments, such as amphotericin-B or pulmonary resection; and a more successful outcome for patients with zygomycosis.

Key Words: zygomycosis, fungal infection, pulmonary vein, hematological disease, computed tomography

(*J Thorac Imaging* 2012;27:W97–W99)

Zygomycosis is caused by the members of the class *Zygomycetes*, including *Mucorales* and *Entomophthorales*, and is known as an invasive infection that occurs in immunocompromised patients, such as those suffering from hematological disorders.[1,2] Recent increased treatment of hematological diseases with chemotherapy coupled with the use of azole antifungal agents for prevention of deep mycosis, such as candidiasis and aspergillosis, has led to the development of zygomycosis with considerable intrinsic resistance to this prophylaxis.[3] Due to this organism's strong ability to invade blood vessels, multiple organs are often involved, and dissemination may occur in affected patients.[1] Pulmonary involvement is seen in approximately 60% of patients and is associated with mortality rates as high as 76%.[4]

Although clinical factors such as underlying diseases, iron overload, and prophylactic use of azole antifungal agents may predispose a patient to zygomycosis, the early diagnosis of this infection is still difficult. It is especially challenging to differentiate it from invasive aspergillosis. Computed tomography (CT) is a powerful tool for the diagnosis of fungal infections.[5] The reported CT manifestations of pulmonary zygomycosis include cavity formation, consolidation, pleural effusion, and pulmonary artery pseudoaneurysm in the advanced stage.[5,6] However, to our knowledge, there is a paucity of literature that describes the radiologic findings of pulmonary zygomycosis with autopsy confirmation. In addition, pulmonary venous invasion, as seen on chest CT, has not been reported as a criterion for the early diagnosis of zygomycosis. From our autopsy files collected over a 4-year period of patients with hematological disease and pulmonary lesions, we reviewed 3 cases with zygomycotic infection to assess for characteristic CT and clinical findings to aid earlier diagnosis.

CASE REPORTS

Case 1

A 61-year-old man with diabetes mellitus and pre-B-cell-type acute lymphoblastic leukemia had a high-grade fever of 38.5°C at admission, and chest x-ray showed parenchymal air space opacity in the left upper lung area. Unenhanced CT scan showed well-defined ground-glass opacity with irregular pulmonary vein dilation in comparison with a previous CT (Figs. 1A, B). His white blood cell (WBC) count was 16800/mm^3, with 74% of blastocytes, and serum *Aspergillus* galactomannan antigen was negative. Despite treatment for 2 weeks with fluconazole and chemotherapy, hemorrhagic brain infarction developed and led to his death. Autopsy confirmed hemorrhagic pulmonary zygomycosis, with fungal hyphae in the pulmonary veins but not in the arteries (Figs. 1C, 2). Cerebral zygomycosis was also found.

Case 2

A 35-year-old man, who had been diagnosed with aplastic anemia at 14 years of age, presented with persistent pancytopenia. Chemotherapy was not effective, and blood transfusions were repeated. After preparative treatment with deferoxamine and fluconazole for hematopoietic stem cell transplantation, high-grade fever of 38.5°C and parenchymal air space opacity in the right upper to middle lung area on chest x-ray appeared. CT scans showed irregular pulmonary vein dilation and bronchial wall thickening surrounded by ground-glass opacity in the right middle lobe compared with previous CT (Fig. 3). His WBC count was 600/mm^3, and serum *Aspergillus* galactomannan antigen was negative. Even after 3 weeks of voriconazole and 1 week of amphotericin-B, respiratory failure progressed and led to his death. Autopsy showed

From the Departments of *Respiratory Medicine; †Clinical Laboratory; ‡Radiology; and §Pathology, Tokyo University Hospital, Bunkyo-ku, Tokyo, Japan.

This manuscript has been read and approved by all authors, who accept full responsibility for its content. All authors had full access to the data and their analysis and participated in the drafting and editing of the article. The authors also declare no conflict of interests regarding the study.

Supported by a research grant from St Luke's Life Science Institute.

Reprints: Hiroshi Kitagawa, MD, PhD, Department of Respiratory Medicine, Tokyo University Hospital, 7-3-1 Hongo, Bunkyo-ku, Tokyo, Japan 113-8655 (e-mail: hkitagawa-tky@umin.ac.jp).